# A factor graph approach to iterative channel estimation, detection and decoding for two-path successive relay networks

Frederic Lehmann

***Abstract*—We consider cooperative communications between a source and a destination node with the help of two relays. In order to overcome the half-duplex constraint, the amplify-and-forward two-path relaying protocol is used. We adopt orthogonal frequency-division multiplexing modulation to combat frequency-selective channels and asynchronous reception at the destination node.**

**In this paper, we develop a coherent receiver architecture suitable for unknown block fading channels. A factor graph representing the joint *a posteriori* probability of the coded symbols and the channels in the frequency domain is introduced. Then, we derive a Bayesian inference algorithm based on message-passing over the factor graph. The resulting iterative receiver maintains low-complexity, based on the interaction between an off-the-shelf soft-input soft-output decoder and a newly introduced per-subcarrier processor for two-path relaying channel estimation and symbol detection. Simulation results show that the proposed solution maintains the full diversity order, even with a limited number of training blocks.**

***Index Terms*—Two-path successive relaying, amplify-and-forward, OFDM, joint channel estimation, detection and decoding, factor graph, message-passing receiver.**

## I. Introduction

Cooperative communications, by forming a virtual antenna array with distant single antenna systems, have the potential to improve the capacity and bit error rate (BER) performance of wireless networks [1]. These performance gains can be exploited to expand the cell range in future 5G wireless communications [2] or to relax the power supply constraints in ad-hoc networks [3].

Although full diversity can be achieved, relays are usually subject to the half-duplex constraint due to radio implementation limitations, which incurs a multiplexing loss [1]. Two-path successive relaying was introduced in [4] as a remedy to this problem. This protocol is based on two half-duplex amplify-and-forward (AF) relays, that alternatively listen and forward messages from a source to a destination node. Consequently, the half-duplex throughput loss is asymptotically recovered [5]. Moreover, several extensions including cooperative spectrum sharing [6], multiple-antenna processing at the destination node [7], using orthogonal spreading codes in consecutive time slots [8] and dual-hop multiple-input multiple-output (MIMO) relaying with more than two relays [9], have been published recently.

However, several important practical issues listed below, have only partially been addressed in the litterature related to AF two-path relaying.

First, initial research on the subject assumed frequency-flat fading channels and perfect timing synchronization between the relay-to-destination and source-to-destination paths [4]-[5]. However, frequency-selective fading channels and asynchronism between the source node and the relays are more realistic in wireless environments. Therefore, we adopt the same solution as in [10], initially proposed for AF two-way cooperative communications. We use orthogonal frequency-division multiplexing (OFDM) modulation, which turns the frequency-selective channel into multiple parallel frequency-flat channels and removes timing errors between signals originating from the source and relays by inserting a long-enough cyclic prefix (CP).

The second issue is that the source and relay transmissions are *a priori* not orthogonal, thus generating inter-relay interference (IRI) [4]-[5]. Therefore in this paper, we will restrict ourselves to the case where directional antennas are available at both relays to eliminate IRI [7], which is feasible for infrastructure-based fixed relays, for instance.

Thirdly, in two-path protocols, the destination receives independent copies of the same information directly from the source, then from one of the relays during subsequent time slots. While this mechanism is essential to provide spatial diversity of order two, it also converts the equivalent source-to-destination link into a channel with memory, due to inter-symbol interference (ISI) [4]-[5]. Extracting the spatial diversity gain thus requires to take the channel memory into account. Efficient hard-output symbol detection methods include the maximum-likelihood sequence estimator (MLSE) [4], [11], iterative serial interference cancellation (SIC) incorporating maximum ratio combining (MRC) [12] and multiuser detection [13]. Soft-input soft-output (SISO) symbol detection based on the BCJR algorithm [14] is also used in [15] for the purpose of iterative detection and decoding.

Fourthly, all aforementioned two-path protocol detection schemes have been studied under perfect channel state information (CSI). However, unreliable source-to-destination (S-D) and composite source-to-relay-to-destination (S-R-D) channel estimates may erode the cooperative diversity gain. It follows that channel estimation is not only an important issue for two-path successive AF relaying, but also a non-trivial task due to

The author is with SAMOVAR, Télécom SudParis, CNRS, Université Paris-Saclay, 9 rue Charles Fourier 91011 EVRY, France (e-mail: frederic.lehmann@it-sudparis.eu).

Phone: (+33) 1 60 76 46 33. Fax: (+33) 1 60 76 44 33

Manuscript received July 10, 2015, revised December 9, 2015 and March 29, 2016.

the superposition of signals originating from the source and relays. Conventional estimation procedures for OFDM-based AF cooperative communications [16]-[17] can also be adapted for two-path relaying, by sounding the channel with three consecutive OFDM training blocks. However, the drawback of such techniques is the implicit assumption that the channel will remain static during subsequent data blocks, until channel sounding is restarted all over again. Similarly to prior work on point-to-point OFDM links [18], there is a need to tackle the problem of faster channel variations in the context of two-way relaying, a goal that was not targeted in previous approaches.

In this paper, we consider the application of the factor graph framework [19]-[20] to two-path successive relaying, for the purpose of Bayesian inference in the frequency-domain. Let us first consider the factor graph for symbol detection and channel estimation. Our focus is on block fading channels, where channel time variations between successive pilot blocks should be explicitly taken into account, on top of the ISI generated by the successive relaying mechanism. Therefore, a mixed discrete-continuous model is requested to model the memory in the network. At the destination node we model the channel time-selectivity and the ISI induced by the direct and alternating relay paths by a first-order Markov model. We show that for a frame of consecutive OFDM blocks, on each subcarrier the detection subgraph corresponding to symbol variables (resp. the channel estimation subgraphs for S-D channel frequency response (CFR) variables and the S-R-D CFR variables) has a simple tree-like structure. Consequently, Bayesian inference of the discrete symbols and the continuous CFR variables based on message-passing, reduces to a per-subcarrier forward-backward procedure on the corresponding subgraphs. Nevertheless, multipath fading induces deep notches in the spectrum of the received signal, thus exposing the corresponding OFDM modulated subcarriers to low signal-to-noise ratios. We apply the classical solution consisting of forward error correction (FEC) coding across subcarriers [21] associated with both time and frequency interleaving. We use codes admitting a factor graph representation, such as convolutional, low-density parity-check or turbo-codes [22]. Now, connecting the factor graphs corresponding respectively to FEC decoding and symbol detection with channel estimation, leads to the complete factor graph. Performing message-passing on the complete factor graph results in an iterative receiver implementing joint channel estimation, symbol detection and decoding for two-path relay networks.

The main technical contributions of this work are

- A bandwidth-efficient two-path successive relaying scheme with a small pilot insertion rate (PIR). Accurate CSI reconstruction between pilot blocks is achieved by using first-order Markov processes to model time-selectivity and by coupling channel estimation with symbol detection and decoding.
- A highly parallelizable, per-subcarrier channel estimation and ISI mitigation scheme. Exploiting assumed conditional independences between observed and unobserved variables, the factor graph representation of the channel estimation and detection problem at hand, exhibits parallel tree-like subgraphs for each subcarrier. Thus message-passing implementation boils down to scalar forward-backward processors activated in parallel for each subcarrier.
- A low-complexity approximate message-passing receiver, inspired from Gaussian belief propagation (GaBP) on Gaussian graphical models [23]. Approximating all continuous-valued messages on the factor graph by Gaussians makes the proposed iterative receiver tractable, by preserving a constant complexity per time recursion and per iteration.

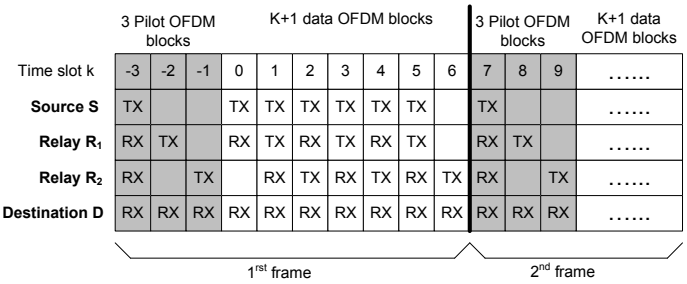


Fig. 1. Frame structure (illustrated for $K = 6$) including: pilot blocks (shaded) and data blocks (unshaded). The AF two-path relaying protocol is represented by the operation of each node: listening (RX), transmitting (TX) or iddle (blank).

Throughout the paper, bold letters indicate vectors and matrices and $\mathcal{N}(x : m, P)$ (resp. $\mathcal{N}_{\mathcal{C}}(x : m, P)$) denotes a real (resp. circularly symmetric complex) Gaussian distribution of the variable $x$, with mean $m$ and variance $P$.

This paper is organized as follows. First, the system model for OFDM modulated amplify-and-forward two-path successive relaying, along with the corresponding factor graph representation, is introduced in Sec. II. The proposed iterative receiver for code-aided ISI mitigation and channel estimation, based on exact message-passing over the factor graph, is derived in Sec. III. A low-complexity alternative, approaching all continuous-valued messages by Gaussian messages is presented in Sec. IV. Finally, in Sec. V, the performances of the proposed iterative receiver are assessed through numerical simulations for the sake of comparison with classical pilot-based and multiuser techniques.

## II. System model

### A. Protocol description

We consider a source node S, that transmits data to a destination node D, with the help of two cooperative relay nodes, $\mathsf{R}_1$ and $\mathsf{R}_2$. All nodes are subject to the half-duplex constraint (i.e. they cannot send and receive at the same time). Each relay is equipped with a directional antenna forming a null in the reception pattern in the direction of the other relay for the purpose of IRI cancellation, while retaining near-omnidirectional coverage over the remaining angles. The source S implements OFDM block transmission, so that the destination D can easily handle channel frequency selectivity and asynchronism [10]. At S, OFDM blocks are arranged in frames containing $K + 4$ consecutive OFDM blocks, among which three (resp. $K + 1$) are devoted to the transmission of the pilot blocks (resp. data blocks). Without loss of generality,

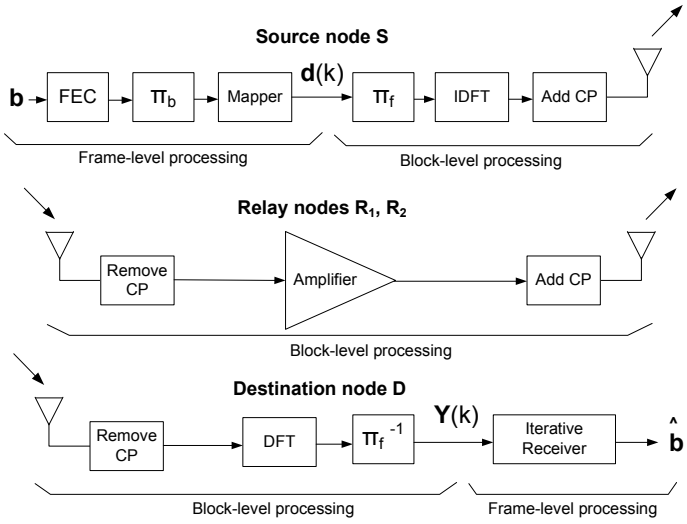


Fig. 2. Architecture of the OFDM-based nodes: source (S), relays ($\mathsf{R}_1$, $\mathsf{R}_2$) and destination (D).

we will consider the first frame in the sequel. Let $k$ denote the index of the time slot devoted to the transmission of each OFDM block at S. As illustrated by Fig. 1, three time slots (corresponding to $k < 0$) are devoted to pilot OFDM blocks, at the the beginning of each frame. The following $K + 1$ time slots, where $K$ is even (corresponding to $k = 0, \ldots, K$) are devoted to data blocks, transmitted using the AF two-path successive relaying protocol. This means that the relays alternatively listen to S and transmit to D, since they cannot do both simultaneously in half-duplex mode [4]-[5]. More precisely, $\mathsf{R}_1$ (resp. $\mathsf{R}_2$) is in a listening phase (resp. in a transmission phase) during even time slots, while during odd time slots its is the other way around. The resulting multiplexing gain given by $K/(K+4)$, approaches 1 when $K$ is sufficiently large. D waits for the $K+1$ OFDM data blocks and the three pilot blocks at the beginning of the current and of the next frame, before it initiates detection and decoding.

### *B. Node architecture*

The baseband signal processing architecture of S, $\mathsf{R}_1$, $\mathsf{R}_2$ and D is depicted in Fig. 2. We let $N$ denote the number of subcarriers per OFDM block and the size of the modulation alphabet is $2^B$.

Let us start with the operations performed by S at the frame level. As stated in Sec. II-A, during a frame S transmits $K$ data blocks, corresponding to a sequence of independently and uniformly distributed information bits, $\mathbf{b}$. To benefit from temporal diversity over the entire frame [24], the binary vector $\mathbf{b}$ is passed to a FEC code, followed by a pseudo-random bit-interleaver $\pi_b(.)$ to obtain the vector of coded bits $\mathbf{c} = [c_1, \ldots, c_{KNB}]$. The deterministic encoding and bit-interleaving function is denoted by

$$\mathbf{c} = \mathcal{C}[\mathbf{b}].$$

The mapper, corresponding to the $2^B$-ary modulation alphabet, partitions $\mathbf{c}$ to length-$N$ vectors of complex data symbols, $\mathbf{d}(k) = [d^0(k), d^1(k), \ldots, d^{N-1}(k)]^T$, where the block index $k = 0, \ldots, K-1$. The deterministic mapping function generating the complex symbol $d^n(k)$ from a set of $B$ binary encoded elements from $\mathbf{c}$ is denoted by

$$d^n(k) = \mathcal{M}^n(k)[\mathbf{c}].$$

The symbol energy after mapping is normalized to $E[|d^n(k)|^2] = 1 \ \forall n, k$. Afterwards, the output of an $N$-point inverse discrete Fourier transform (IDFT) fed with $\mathbf{d}(k)$ scrambled by a frequency (subcarrier) interleaver $\pi_f(.)$, preceeded by a length-$G$ cyclic prefix (CP), forms the $k$-th transmitted OFDM block. Note that frequency interleaving is used in order to exploit the frequency diversity induced by multipath propagation [24].

Now, we define the block-level relay processing. Let us consider the transmission link from node A to node B, $E_{\mathsf{AB}}$ denotes the average symbol energy at the receiving antenna of node B. The additive white Gaussian noise (AWGN) samples at the receive antenna of each node, are independently and identically distributed (i.i.d.) according to a zero-mean complex Gaussian distribution with variance $N_0$. To keep relay processing simple, AF is implemented. In order to reduce the required CP length, during a relay's listening phase, an OFDM block transmitted by S is overheard and undergoes CP removal, amplification and new CP insertion [10]. This technique removes the inter-block interference (IBI) (confined inside the CP) altogether at relay $\mathsf{R}_\mathsf{i}$ [10], so that the effective length of the compound S-$\mathsf{R}_\mathsf{i}$-D CIR at D becomes $L$, instead of $2L-1$ for the concurrent method where $\mathsf{R}_\mathsf{i}$ applies AF to the CP as well. At $\mathsf{R}_1$ (resp. $\mathsf{R}_2$) the amplifier gain factor is $\beta_{\mathsf{R}_1} = \sqrt{E_{\mathsf{R}_1\mathsf{D}}}/\sqrt{E_{\mathsf{SR}_1} + N_0}$ (resp. $\beta_{\mathsf{R}_2} = \sqrt{E_{\mathsf{R}_2\mathsf{D}}}/\sqrt{E_{\mathsf{SR}_2} + N_0}$), in order to renormalize the symbol energy to $E_{\mathsf{R}_1\mathsf{D}}$ (resp. $E_{\mathsf{R}_2\mathsf{D}}$). These operations induce a latency of one OFDM symbol. During a relay's transmission phase, the currently available OFDM signal is re-radiated towards D. Here, we assume that each relay is equipped with a directional antenna that receives signals originating only from S, while completely eliminating IRI.

Finally, let us describe the block-level frequency-domain processing performed at the destination D. After CP removal, the $k$-th OFDM block received from S, superposed with the signal sent by $\mathsf{R}_1$ or $\mathsf{R}_2$, is transformed by an $N$-point discrete Fourier transform (DFT) followed by frequency de-interleaving into a noisy observation vector $\mathbf{Y}(k) = [Y^0(k), Y^1(k), \ldots, Y^{N-1}(k)]^T$, which is in turn fed to the proposed iterative receiver for data recovery at the frame level.

### *C. Channel model*

We assume all nodes to be sufficiently far appart in space so that the channel impulse response (CIR) of all existing wireless links are statistically independent [26]. Assuming a rich multipath scattering environment, during the $k$-th time slot, the discrete CIR between any two nodes A and B is represented by a length-$L$ vector of independent zero-mean complex Gaussian channel coefficients [25], $\mathbf{h}_{\mathsf{A},\mathsf{B}}(k) = [h^0_{\mathsf{A},\mathsf{B}}(k), \ldots, h^{L-1}_{\mathsf{A},\mathsf{B}}(k)]^T$. For convenience, the power of the $L$ coefficients are normalized, such that $\sum_{l=0}^{L-1} E[|h^l_{\mathsf{A},\mathsf{B}}(k)|^2] =$

1. We assume block fading, that is channel coefficients remain constant during each OFDM block, but can vary from one block to the next according to a Markov model. Let $\{H^m_{\mathsf{A,B}}(k)\}_{m=0}^{N-1}$ denote the channel frequency response (CFR) between node A and node B during the $k$-th time slot. Then $\{H^m_{\mathsf{A,B}}(k)\}_{m=0}^{N-1}$ is the $N$-point DFT of the zero-padded CIR $\mathbf{h}_{\mathsf{A,B}}(k)$.

### *D. Observation model*

At the destination node D, the received block during the $k$-th time slot is the superposition of signals sent by S and by one of the relays, respectively. These signals have different timing offsets due to different propagation delays, which may cause IBI. As shown in [10], a long enough CP will solve this problem. Furthermore, the superposed signals impinging at D have the same carrier frequency offset (CFO), since AF relaying is used. Consequently, conventional single-user OFDM timing and CFO compensation are in order [27]. In the sequel, we will assume no residual IBI due to asynchronism (perfect timing synchronization) and ideal CFO compensation at D, so that subcarrier orthogonality is preserved.

We consider the frequency-domain received signal at D, i.e. after CP removal, $N$-point DFT and frequency de-interleaving:

*1) If the time slot $k$ is even:* On the $n$-th subcarrier corresponding to the transmission of $d^n(k)$, $n = 0, \ldots, N-1$, D receives

$$\begin{aligned} Y^n(k) =& \sqrt{E_{\mathsf{SD}}} H_{\mathsf{SD}}^{\pi_f^{-1}(n)}(k) d^n(k) + \\ & \sqrt{E_{\mathsf{SR}_2}} \beta_{\mathsf{R}_2} H_{\mathsf{SR}_2}^{\pi_f^{-1}(n)}(k-1) H_{\mathsf{R}_2\mathsf{D}}^{\pi_f^{-1}(n)}(k) d^n(k-1) + \\ & z_{\mathsf{e}}^n(k), \end{aligned} \tag{1}$$

where the first (resp. second) term stems from the signal directly received from S (resp. received from $\mathsf{R}_2$). The third term is the noise contribution, which is the sum of the noise at D during the current time slot and the noise forwarded by $\mathsf{R}_2$ during the previous time slot. These noise terms being independent, $z_{\mathsf{e}}^n(k)$ is i.i.d. noise, whose distribution can approximated as $\mathcal{N}_C(z_{\mathsf{e}}^n(k) : 0, R_{\mathsf{e}})$, where $R_{\mathsf{e}} = (\beta_{\mathsf{R}_2}^2 + 1) N_0$.

*Remark 2.1:* Note that according to Fig. 1, a slight modification is needed for the particular time slots $k = 0$ and $k = K + 1$. When $k = 0$ only the first signal component and the noise contribution at D exist. Conversely, when $k = K + 1$ only the second signal component while both the noise contribution at D and the one forwarded by $\mathsf{R}_2$ exist.

*2) If the time slot $k$ is odd:* On the $n$-th subcarrier corresponding to the transmission of $d^n(k)$, $n = 0, \ldots, N-1$, D receives

$$\begin{aligned} Y^n(k) =& \sqrt{E_{\mathsf{SD}}} H_{\mathsf{SD}}^{\pi_f^{-1}(n)}(k) d^n(k) + \\ & \sqrt{E_{\mathsf{SR}_1}} \beta_{\mathsf{R}_1} H_{\mathsf{SR}_1}^{\pi_f^{-1}(n)}(k-1) H_{\mathsf{R}_1\mathsf{D}}^{\pi_f^{-1}(n)}(k) d^n(k-1) + \\ & z_{\mathsf{o}}^n(k), \end{aligned} \tag{2}$$

where the first (resp. second) term stems from the signal directly received from S (resp. received from $\mathsf{R}_1$). The third term $z_{\mathsf{o}}^n(k)$, is the i.i.d. noise contribution, whose distribution can approximated as $\mathcal{N}_C(z_{\mathsf{o}}^n(k) : 0, R_{\mathsf{o}})$ with $R_{\mathsf{o}} = (\beta_{\mathsf{R}_1}^2 + 1) N_0$.

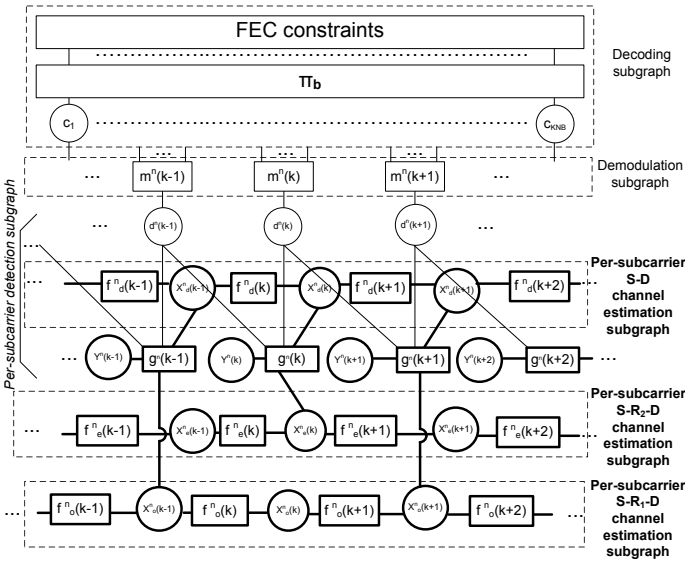


Fig. 3. Factor graph corresponding to receiver processing at the destination node D. Here the time slot index $k$ is assumed even.

For ease of exposition, we introduce the following CFR notations for the $k$-th time slot on the $n$-th subcarrier

$$\begin{aligned} X_{\mathsf{d}}^n(k) &= \sqrt{E_{\mathsf{SD}}} H_{\mathsf{SD}}^{\pi_f^{-1}(n)}(k) \\ X_{\mathsf{e}}^n(k) &= \sqrt{E_{\mathsf{SR}_2}} \beta_{\mathsf{R}_2} H_{\mathsf{SR}_2}^{\pi_f^{-1}(n)}(k-1) H_{\mathsf{R}_2\mathsf{D}}^{\pi_f^{-1}(n)}(k) \\ X_{\mathsf{o}}^n(k) &= \sqrt{E_{\mathsf{SR}_1}} \beta_{\mathsf{R}_1} H_{\mathsf{SR}_1}^{\pi_f^{-1}(n)}(k-1) H_{\mathsf{R}_1\mathsf{D}}^{\pi_f^{-1}(n)}(k). \end{aligned} \tag{3}$$

The first line corresponds to the CFR of the direct S-D link. The second (resp. third) line corresponds to the composite CFR of the S-$\mathsf{R}_2$-D (resp. S-$\mathsf{R}_1$-D) link, which appears during even (resp. odd) time slots. Using the Rayleigh fading and link independence assumptions of Sec. II-C, we can find the prior distribution of the elements in (3). The prior distribution of $X_{\mathsf{d}}^n(k)$ is circularly symmetric complex Gaussian with parameters

$$\begin{aligned} & E\left[X_{\mathsf{d}}^n(k)\right] = 0 \\ & E\left[\left|X_{\mathsf{d}}^n(k)\right|^2\right] = E_{\mathsf{SD}}, \end{aligned} \tag{4}$$

and the prior distribution of $X_{\mathsf{e}}^n(k)$ and $X_{\mathsf{o}}^n(k)$ is a complex double Gaussian distribution [28], whose first two moments are

$$\begin{aligned} & E\left[X_{\mathsf{e}}^n(k)\right] = E\left[X_{\mathsf{o}}^n(k)\right] = 0 \\ & E\left[\left|X_{\mathsf{e}}^n(k)\right|^2\right] = E_{\mathsf{SR}_2} \beta_{\mathsf{R}_2}^2 \\ & E\left[\left|X_{\mathsf{o}}^n(k)\right|^2\right] = E_{\mathsf{SR}_1} \beta_{\mathsf{R}_1}^2. \end{aligned} \tag{5}$$

### *E. Factor graph representation*

A factor graph is a convenient visualization of the factorization of a global function into a product of local functions, depending on a subset of the arguments also called variables [19]-[20]. Marginals of the global function can then be efficiently computed using the sum-product algorithm [19]-[20], which consists in message-passing over the factor graph. Since our primary interest focuses on Bayesian inference of CFRs and the encoded bits, we choose the global function as

the *a posteriori* probability density function (p.d.f.) of interest, while the variables are the unobserved and observed variables defined previously.

At the destination node D, the unobserved variables contain continuous variables, such as the CFRs defined in (3)

$$\mathbf{X}_{\mathsf{d}} = \{X_{\mathsf{d}}^n(k)\}_{\substack{n=0,\ldots,N-1,\\ k=0,\ldots,K-1}}$$
$$\mathbf{X}_{\mathsf{e}} = \{X_{\mathsf{e}}^n(k)\}_{\substack{n=0,\ldots,N-1,\\ k=1,\ldots,K}}$$
$$\mathbf{X}_{\mathsf{o}} = \{X_{\mathsf{o}}^n(k)\}_{\substack{n=0,\ldots,N-1,\\ k=0,\ldots,K-1}}$$

as well as discrete variables, such as the modulated data,

$$\mathbf{D} = \{d^n(k)\}_{\substack{n=0,\ldots,N-1,\\ k=0,\ldots,K-1}}$$

the encoded bit stream, $\mathbf{c}$ and the uncoded bit stream, $\mathbf{b}$. The observed variables are the corrresponding noisy observations, collected by D during even and odd time slots

$$\mathbf{Y} = \{Y^n(k)\}_{\substack{n=0,\ldots,N-1,\\ k=0,\ldots,K}} \quad .$$

Therefore, the posterior p.d.f. of interest has the form

$$\begin{aligned} &p\left(\mathbf{X}_{\mathsf{d}}, \mathbf{X}_{\mathsf{e}}, \mathbf{X}_{\mathsf{o}}, \mathbf{D}, \mathbf{c}, \mathbf{b} | \mathbf{Y}\right) \\ &\propto p\left(\mathbf{Y} | \mathbf{X}_{\mathsf{d}}, \mathbf{X}_{\mathsf{e}}, \mathbf{X}_{\mathsf{o}}, \mathbf{D}\right) p(\mathbf{X}_{\mathsf{d}}) p(\mathbf{X}_{\mathsf{e}}) p(\mathbf{X}_{\mathsf{o}}) p(\mathbf{D}|\mathbf{c}) p(\mathbf{c}|\mathbf{b}) p(\mathbf{b}), \end{aligned}$$

where the second line in obtained from Bayes's rule, the fact that channels for different links are independent (see Sec. II-C) and the independence between the data and the channels. Using the memoryless channel assumption due to subcarrier orthogonality and noise independence (see Sec. II-D), $p\left(\mathbf{Y} | \mathbf{X}_{\mathsf{d}}, \mathbf{X}_{\mathsf{e}}, \mathbf{X}_{\mathsf{o}}, \mathbf{D}\right)$ factorizes into

$$\begin{aligned} &p\left(\mathbf{Y} | \mathbf{X}_{\mathsf{d}}, \mathbf{X}_{\mathsf{e}}, \mathbf{X}_{\mathsf{o}}, \mathbf{D}\right) \\ &= \prod_{n=0}^{N-1} \Big\{ p(Y^n(0) | X_{\mathsf{d}}^n(0), d^n(0)) \\ &\qquad \times \prod_{\substack{k=2 \\ k \text{ even}}}^{K-2} p(Y^n(k) | X_{\mathsf{d}}^n(k), X_{\mathsf{e}}^n(k), d^n(k-1), d^n(k)) \\ &\qquad \times \prod_{\substack{k=1 \\ k \text{ odd}}}^{K-1} p(Y^n(k) | X_{\mathsf{d}}^n(k), X_{\mathsf{o}}^n(k), d^n(k-1), d^n(k)) \\ &\qquad \times p(Y^n(K) | X_{\mathsf{e}}^n(K), d^n(K-1)) \Big\}. \end{aligned}$$

Now, exploiting the first-order Markov block fading assumption of Sec. II-C and assuming that $\pi_f(.)$ implements ideal frequency interleaving, we obtain the factorizations

$$\begin{aligned} p(\mathbf{X}_{\mathsf{d}}) &= \prod_{n=0}^{N-1} \Big\{ p(X_{\mathsf{d}}^n(0) \prod_{k=1}^{K-1} p(X_{\mathsf{d}}^n(k) | X_{\mathsf{d}}^n(k-1)) \Big\} \\ p(\mathbf{X}_{\mathsf{e}}) &= \prod_{n=0}^{N-1} \Big\{ p(X_{\mathsf{e}}^n(1) \prod_{k=2}^{K} p(X_{\mathsf{e}}^n(k) | X_{\mathsf{e}}^n(k-1)) \Big\} \\ p(\mathbf{X}_{\mathsf{o}}) &= \prod_{n=0}^{N-1} \Big\{ p(X_{\mathsf{o}}^n(0) \prod_{k=1}^{K-1} p(X_{\mathsf{o}}^n(k) | X_{\mathsf{o}}^n(k-1)) \Big\}. \end{aligned} \tag{6}$$

Finally, exploiting the fact that mapping and encoding/bit-interleaving functions are deterministic, we obtain

$$\begin{aligned} p(\mathbf{D}|\mathbf{c}) &\propto \prod_{n=0}^{N-1} \prod_{k=0}^{K-1} I\left(d^n(k) = \mathcal{M}^n(k)[\mathbf{c}]\right) \\ p(\mathbf{c}|\mathbf{b}) &\propto I(\mathbf{c} = \mathcal{C}[\mathbf{b}]), \end{aligned}$$

where $I(.)$ denotes the indicator function. Furthermore, since $\mathbf{b}$ is uniformly distributed according to Sec. II-B, $p(\mathbf{b})$ is an irrelevant constant, which plays no role in the factor graph. The factor graph corresponding to the above factorizations is depicted in Fig. 3. Without loss of generality, in Fig. 3, the $k$-th (resp. $k-1$-th or $k+1$-th) transmission correspond to an even (resp. odd) time slot. Variable nodes are represented as circles and the local functions appearing in the factorization, denoted by

$$\begin{aligned} m^n(k) &= I\left(d^n(k) = \mathcal{M}^n(k)[\mathbf{c}]\right) \\ f_{\mathsf{d}}^n(k) &= p(X_{\mathsf{d}}^n(k) | X_{\mathsf{d}}^n(k-1)) \\ f_{\mathsf{e}}^n(k) &= p(X_{\mathsf{e}}^n(k) | X_{\mathsf{e}}^n(k-1)) \\ f_{\mathsf{o}}^n(k) &= p(X_{\mathsf{o}}^n(k) | X_{\mathsf{o}}^n(k-1)) \\ g^n(k) &= \begin{cases} p(Y^n(k) | X_{\mathsf{d}}^n(k), X_{\mathsf{e}}^n(k), d^n(k-1), d^n(k)), & k \text{ even} \\ p(Y^n(k) | X_{\mathsf{d}}^n(k), X_{\mathsf{o}}^n(k), d^n(k-1), d^n(k)), & k \text{ odd} \end{cases} \end{aligned} \tag{7}$$

are represented as squares. We notice that the resulting factor graph can be decomposed into several subgraphs corresponding to distinct Bayesian estimation tasks. All subgraphs below the complex data symbols are tree-like per-subcarrier subgraphs, including CFR estimation subgraphs in the background (bold) and the zig-zag data detection subgraph in the foreground (light). Note that only per-subcarrier subgraphs related to the previously defined $n$-th subcarrier are depicted in Fig. 3. Therefore, it is understood that all per-subcarrier subgraphs related to other subcarriers have exactly the same structure and should be depicted in parallel perspective (which we refrain from doing here, in order not to overload the figure). Conversely, above the complex data symbols, an across all subcarriers subgraph appears, that corresponds to the local function $I(\mathbf{c} = \mathcal{C}[\mathbf{b}])$, or in other words to bit-interleaving and FEC constraints. As expected, the demodulation subgraphs form the interface between per sub-carrier subgraphs and the across all subcarriers subgraph.

## III. Exact form of the message-passing receiver

We assume that the reader is familiar with the factor graph framework [19]-[20]. The goal of the proposed Bayesian receiver is to estimate the CFRs, detect the data symbols and decode the message bits at the receiver side. Using the factor graph framework will greatly facilitate these tasks, which reduce to propagating messages along the edges of the factor graph using the sum-product rule [19]-[20]. We now turn our attention to deriving the exact expression of those messages on each subgraph. We let $\mu_{u \to v}(.)$ denote the message sent by node $u$ to node $v$ in the factor graph.

### A. Per-subcarrier S-D CFR estimation subgraph

The incoming messages on the S-D CFR estimation subgraph are computed from the sum-product rule applied at the factor node $g^n(k)$

$$\begin{aligned}&\mu_{g^n(k)\to X_{\mathsf{d}}^n(k)}(X_{\mathsf{d}}^n(k))\\ &\propto \sum_{d^n(k-1)}\sum_{d^n(k)} \mu_{d^n(k-1)\to g^n(k)}(d^n(k-1))\\ &\quad\times \mu_{d^n(k)\to g^n(k)}(d^n(k))\\ &\quad\times \int p\left(Y^n(k)|X_{\mathsf{d}}^n(k),X_{\mathsf{e}}^n(k),d^n(k-1),d^n(k)\right)\\ &\qquad\times \mu_{X_{\mathsf{e}}^n(k)\to g^n(k)}(X_{\mathsf{e}}^n(k))dX_{\mathsf{e}}^n(k),\end{aligned} \tag{8}$$

which acts as a the likelihood of $Y^n(k)$ given $X_{\mathsf{d}}^n(k)$, where the discrete symbols $d^n(k-1)$, $d^n(k)$ and the CFR variable $X_{\mathsf{e}}^n(k)$ are marginalized out. Now let us compute the messages in the forward direction

$$\begin{aligned}&\mu_{f_{\mathsf{d}}^n(k+1)\to X_{\mathsf{d}}^n(k+1)}(X_{\mathsf{d}}^n(k+1))\\ &\propto \int p(X_{\mathsf{d}}^n(k+1)|X_{\mathsf{d}}^n(k))\mu_{g^n(k)\to X_{\mathsf{d}}^n(k)}(X_{\mathsf{d}}^n(k))\\ &\qquad\times \mu_{f_{\mathsf{d}}^n(k)\to X_{\mathsf{d}}^n(k)}(X_{\mathsf{d}}^n(k))dX_{\mathsf{d}}^n(k),\end{aligned} \tag{9}$$

which has the form of a recursive Bayesian filter. The messages in the backward direction follow a similar backward Bayesian filter recursion

$$\begin{aligned}&\mu_{f_{\mathsf{d}}^n(k)\to X_{\mathsf{d}}^n(k-1)}(X_{\mathsf{d}}^n(k-1))\\ &\propto \int p(X_{\mathsf{d}}^n(k)|X_{\mathsf{d}}^n(k-1))\mu_{g^n(k)\to X_{\mathsf{d}}^n(k)}(X_{\mathsf{d}}^n(k))\\ &\qquad\times \mu_{f_{\mathsf{d}}^n(k+1)\to X_{\mathsf{d}}^n(k)}(X_{\mathsf{d}}^n(k))dX_{\mathsf{d}}^n(k).\end{aligned} \tag{10}$$

Now let us turn our attention to the outgoing messages from the S-D CFR estimation subgraph. Applying the sum-product rule at the variable node $X_{\mathsf{d}}^n(n)$, we obtain

$$\begin{aligned}&\mu_{X_{\mathsf{d}}^n(k)\to g^n(k)}(X_{\mathsf{d}}^n(k))\\ &\quad\propto \mu_{f_{\mathsf{d}}^n(k)\to X_{\mathsf{d}}^n(k)}(X_{\mathsf{d}}^n(k))\mu_{f_{\mathsf{d}}^n(k+1)\to X_{\mathsf{d}}^n(k)}(X_{\mathsf{d}}^n(k)),\end{aligned} \tag{11}$$

which, as a product of forward and backward expressions recursively obtained in (9) and (10), acts as a Bayesian smoothing equation.

*Remark 3.1:* All expressions are valid for $k$ even as in Fig. 3. If $k$ is odd, the messages keep the same expression, but replacing the subscripts $\mathsf{e}$ by $\mathsf{o}$.

*Remark 3.2:* Note that since the S-D CFR estimation subgraphs for all subcarriers are disconnected, the message-passing algorithm (8)-(11) can be executed in parallel for all subcarrier indices $n = 0, \ldots, N-1$.

### B. Per-subcarrier S-R$_2$-D CFR estimation subgraph

First let us examine the incoming messages on the S-R$_2$-D CFR estimation subgraph. The sum-product rule applied at the factor node $g^n(k)$ results in

$$\begin{aligned}&\mu_{g^n(k)\to X_{\mathsf{e}}^n(k)}(X_{\mathsf{e}}^n(k))\\ &\propto \sum_{d^n(k-1)}\sum_{d^n(k)} \mu_{d^n(k-1)\to g^n(k)}(d^n(k-1))\\ &\quad\times \mu_{d^n(k)\to g^n(k)}(d^n(k))\\ &\quad\times \int p\left(Y^n(k)|X_{\mathsf{d}}^n(k),X_{\mathsf{e}}^n(k),d^n(k-1),d^n(k)\right)\\ &\qquad\times \mu_{X_{\mathsf{d}}^n(k)\to g^n(k)}(X_{\mathsf{d}}^n(k))dX_{\mathsf{d}}^n(k),\end{aligned} \tag{12}$$

where $\mu_{X_{\mathsf{d}}^n(k)\to g^n(k)}(X_{\mathsf{d}}^n(k))$ is readily available from (11). (12) acts as a the likelihood of $Y^n(k)$ given $X_{\mathsf{e}}^n(k)$, where the discrete symbols $d^n(k-1)$, $d^n(k)$ and the CFR variable $X_{\mathsf{d}}^n(k)$ are marginalized out. During even time slots, the message in the forward direction is

$$\begin{aligned}&\mu_{f_{\mathsf{e}}^n(k+1)\to X_{\mathsf{e}}^n(k+1)}(X_{\mathsf{e}}^n(k+1))\\ &\propto \int p(X_{\mathsf{e}}^n(k+1)|X_{\mathsf{e}}^n(k))\mu_{g^n(k)\to X_{\mathsf{e}}^n(k)}(X_{\mathsf{e}}^n(k))\\ &\qquad\times \mu_{f_{\mathsf{e}}^n(k)\to X_{\mathsf{e}}^n(k)}(X_{\mathsf{e}}^n(k))dX_{\mathsf{e}}^n(k)\end{aligned} \tag{13}$$

while during odd time slots it reduces to the prediction integral

$$\begin{aligned}&\mu_{f_{\mathsf{e}}^n(k)\to X_{\mathsf{e}}^n(k)}(X_{\mathsf{e}}^n(k))\\ &\propto \int p(X_{\mathsf{e}}^n(k)|X_{\mathsf{e}}^n(k-1))\\ &\qquad\times \mu_{f_{\mathsf{e}}^n(k-1)\to X_{\mathsf{e}}^n(k-1)}(X_{\mathsf{e}}^n(k-1))dX_{\mathsf{e}}^n(k-1)\end{aligned} \tag{14}$$

in the absence of observation on $X_{\mathsf{e}}^n(k-1)$.

Similarly, during even time slots, the message in the backward direction is

$$\begin{aligned}&\mu_{f_{\mathsf{e}}^n(k)\to X_{\mathsf{e}}^n(k-1)}(X_{\mathsf{e}}^n(k-1))\\ &\propto \int p(X_{\mathsf{e}}^n(k)|X_{\mathsf{e}}^n(k-1))\mu_{g^n(k)\to X_{\mathsf{e}}^n(k)}(X_{\mathsf{e}}^n(k))\\ &\qquad\times \mu_{f_{\mathsf{e}}^n(k+1)\to X_{\mathsf{e}}^n(k)}(X_{\mathsf{e}}^n(k))dX_{\mathsf{e}}^n(k)\end{aligned} \tag{15}$$

while during odd time slots it reduces to the prediction integral

$$\begin{aligned}&\mu_{f_{\mathsf{e}}^n(k+1)\to X_{\mathsf{e}}^n(k)}(X_{\mathsf{e}}^n(k))\\ &\propto \int p(X_{\mathsf{e}}^n(k+1)|X_{\mathsf{e}}^n(k))\\ &\qquad\times \mu_{f_{\mathsf{e}}^n(k+2)\to X_{\mathsf{e}}^n(k+1)}(X_{\mathsf{e}}^n(k+1))dX_{\mathsf{e}}^n(k+1)\end{aligned} \tag{16}$$

in the absence of observation on $X_{\mathsf{e}}^n(k+1)$. Furthermore the outgoing messages from the S-R$_2$-D CFR estimation subgraph are computed from the smoothing equation

$$\begin{aligned}&\mu_{X_{\mathsf{e}}^n(k)\to g^n(k)}(X_{\mathsf{e}}^n(k))\\ &\quad\propto \mu_{f_{\mathsf{e}}^n(k)\to X_{\mathsf{e}}^n(k)}(X_{\mathsf{e}}^n(k))\mu_{f_{\mathsf{e}}^n(k+1)\to X_{\mathsf{e}}^n(k)}(X_{\mathsf{e}}^n(k)),\end{aligned} \tag{17}$$

obtained from the sum-product rule applied at the variable node $X_{\mathsf{e}}^n(k)$.

Again, the messages for all subcarriers can be calculated in parallel.

### C. Per-subcarrier S-R$_1$-D CFR estimation subgraph

The S-R$_1$-D CFR estimation subgraph structure is exactly the same as the one exploited for S-R$_2$-D CFR estimation in Sec. III-B, with an offset of one time slot. Therefore, details of message calculations are omitted here.

### D. Per-subcarrier detection subgraph

Message-passing on the per-subcarrier detection subgraphs is a crutial step, since it allows to take into account the memory-1 ISI generated by the two-path protocol and in turn to extract the available spatial diversity. Assume that the input messages to the detection subgraph, $\mu_{m^n(k)\to d^n(k)}(d^n(k))$, for $k=0,\ldots,K-1$ are available. We will elaborate further on these messages in Sec. III-E.

Applying the sum-product rule at the constraint node $g^n(k)$, we obtain again a forward recursion

$$\begin{aligned}
&\mu_{g^n(k)\to d^n(k)}(d^n(k))\\
&\propto \sum_{d^n(k-1)} \mu_{g^n(k-1)\to d^n(k-1)}(d^n(k-1))\\
&\quad\times \mu_{m^n(k-1)\to d^n(k-1)}(d^n(k-1))\\
&\quad\times \int\int p\left(Y^n(k)|X_{\mathsf{d}}^n(k),X_{\mathsf{e}}^n(k),d^n(k-1),d^n(k)\right)\\
&\qquad\times \mu_{X_{\mathsf{d}}^n(k)\to g^n(k)}(X_{\mathsf{d}}^n(k))\\
&\qquad\times \mu_{X_{\mathsf{e}}^n(k)\to g^n(k)}(X_{\mathsf{e}}^n(k))dX_{\mathsf{d}}^n(k)dX_{\mathsf{e}}^n(k),
\end{aligned} \tag{18}$$

where $\mu_{X_{\mathsf{d}}^n(k)\to g^n(k)}(X_{\mathsf{d}}^n(k))$ and $\mu_{X_{\mathsf{e}}^n(k)\to g^n(k)}(X_{\mathsf{e}}^n(k))$ are readily available from (11) and (17), respectively. The double integral in (18) acts as a the likelihood of $Y^n(k)$ given $d^n(k-1)$ and $d^n(k)$, where all CFR variables are marginalized out. Now, applying the sum-product rule at the constraint node $g^n(k+1)$, a similar backward recursion is obtained as

$$\begin{aligned}
&\mu_{g^n(k+1)\to d^n(k)}(d^n(k))\\
&\propto \sum_{d^n(k+1)} \mu_{g^n(k+2)\to d^n(k+1)}(d^n(k+1))\\
&\times \mu_{m^n(k+1)\to d^n(k+1)}(d^n(k+1))\\
&\times \int\int p\left(Y^n(k+1)|X_{\mathsf{d}}^n(k+1),X_{\mathsf{o}}^n(k+1),d^n(k),d^n(k+1)\right)\\
&\qquad\times \mu_{X_{\mathsf{d}}^n(k+1)\to g^n(k+1)}(X_{\mathsf{d}}^n(k+1))\\
&\qquad\times \mu_{X_{\mathsf{o}}^n(k+1)\to g^n(k+1)}(X_{\mathsf{o}}^n(k+1))dX_{\mathsf{d}}^n(k+1)dX_{\mathsf{o}}^n(k+1).
\end{aligned} \tag{19}$$

The double integral in (19) acts as a the likelihood of $Y^n(k+1)$ given $d^n(k)$ and $d^n(k+1)$, where all CFR variables are marginalized out. As a by-product, we also obtain the symbol-level probabilities required in (8) and (12) as

$$\begin{aligned}
&\mu_{d^n(k-1)\to g^n(k)}(d^n(k-1)) =\\
&\mu_{g^n(k-1)\to d^n(k-1)}(d^n(k-1))\mu_{m^n(k-1)\to d^n(k-1)}(d^n(k-1)),\\
&\mu_{d^n(k)\to g^n(k)}(d^n(k)) =\\
&\mu_{g^n(k+1)\to d^n(k)}(d^n(k))\mu_{m^n(k)\to d^n(k)}(d^n(k)).
\end{aligned} \tag{20}$$

Finally, the outgoing messages towards the demodulation subgraph are obtained from the sum-product rule applied at $d^n(k)$ as

$$\begin{aligned}
&\mu_{d^n(k)\to m^n(k)}(d^n(k))\\
&\propto\mu_{g^n(k)\to d^n(k)}(d^n(k))\mu_{g^n(k+1)\to d^n(k)}(d^n(k)).
\end{aligned} \tag{21}$$

The obtained messages are reminiscent of the message-passing equalizer developed in [29], which was shown to be optimal for memory-1 ISI channels in the perfect CSI case. Our equations (18)-(21) form an extension of this algorithm, for the case of a memory-1 ISI channel whose CSI is itself obtained through the messages calculated in Sec. III-A, III-B and III-C.

*Remark 3.3:* All expressions are valid for $k$ even as in Fig. 3. If $k$ is odd, the messages keep the same expression, but swapping the subscripts e and o.

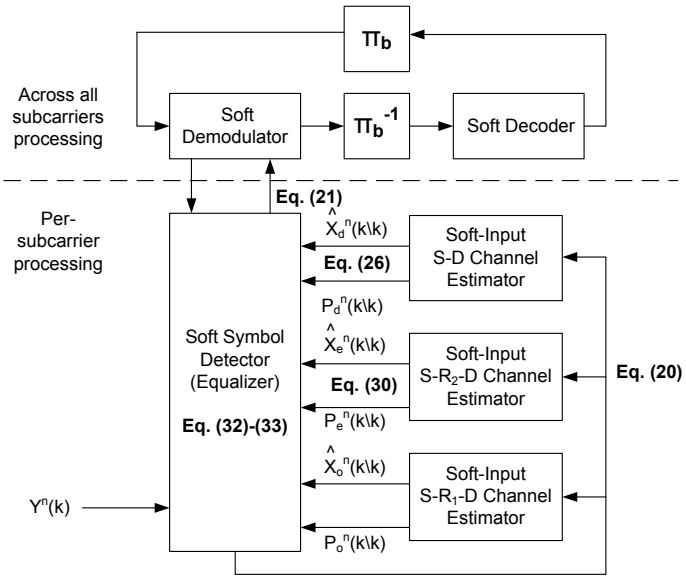


Fig. 4. Proposed low-complexity iterative receiver.

### E. Demodulation and decoding subgraph

The messages of the form (21) act as symbol probabilities at the output of a virtual memory-1 ISI channel. The messages in the opposite direction, i.e. $\mu_{m^n(k)\to d^n(k)}(d^n(k))$, for $k=0,\ldots,K-1$ and $n=0,\ldots,N-1$, can be interpreted as *extrinsic* symbol probabilities obtained from the *extrinsic* bit probabiblities computed by the decoder. The justification is that those probabilities are the input and ouput of a belief propagation algorithm performed on the demodulation and decoding subgraph, which boils down to standard turbo-demodulation. Thus, no further development is needed here. The interested reader can find the details in [30].

## IV. Low-complexity message-passing receiver

The receiver derived in Sec. III, though the exact form of the message-passing algorithm, is not amenable to a closed form solution. This problem is solved under the Gaussian process assumption introduced in Sec. IV-A for all CFRs. However, even with this simplification, the computational problem remains unsolved, since the continuous-valued messages are now in the form of Gaussian mixtures, whose number of mixands grows with time and the iteration index. In order to specify an algorithm that can be implemented in practice, we propose a second simplification in Sec. IV-B-IV-D, which consists in collapsing all continuous-valued messages into a single Gaussian at each instant and at each iteration. Without using any further approximation, the analytic expression of the discrete-valued messages useful for detection and decoding, is obtained in Sec. IV-E-IV-F. Fig. 4 illustrates the interactions between the components of the proposed low-complexity iterative receiver, with references to equation numbers in the text.

### A. CFR state-space model

According to Sec. II-C, Markovian block fading is assumed for the temporal variations of all channel links. Since ideal frequency interleaving is assumed, we adopt independent random walk models [31] for all subcarrier indices $n = 0, \ldots, N-1$

$$\begin{cases} X_{\mathsf{d}}^n(k) = X_{\mathsf{d}}^n(k-1) + \Delta u_{\mathsf{d}}^n(k) \\ X_{\mathsf{e}}^n(k) = X_{\mathsf{e}}^n(k-1) + \Delta u_{\mathsf{e}}^n(k) \\ X_{\mathsf{o}}^n(k) = X_{\mathsf{o}}^n(k-1) + \Delta u_{\mathsf{o}}^n(k) \end{cases} \tag{22}$$

where $\Delta u_{\mathsf{d}}^n(k) \sim \mathcal{N}_C(\Delta u_{\mathsf{d}}^n(k) : 0, q_{\mathsf{d}})$, $\Delta u_{\mathsf{e}}^n(k) \sim \mathcal{N}_C(\Delta u_{\mathsf{e}}^n(k) : 0, q_{\mathsf{e}})$ and $\Delta u_{\mathsf{o}}^n(k) \sim \mathcal{N}_C(\Delta u_{\mathsf{o}}^n(k) : 0, q_{\mathsf{o}})$ are i.i.d. Gaussian driving noises. The parameter $q_{\mathsf{d}}$ (resp. $q_{\mathsf{e}}$ and $q_{\mathsf{o}}$) must be optimized based on the coherence time [25] of the S-D (resp. the composite S-R$_2$-D and composite S-R$_1$-D) channel CFR. An initialization in the form of a prior distribution for $X_{\mathsf{d}}^n(0)$ and $X_{\mathsf{e}}^n(1)$ and $X_{\mathsf{o}}^n(0)$ is needed, which is chosen as the circularly symmetric complex Gaussian with parameters given by (4)-(5). It follows that the CFRs in (3) are modeled as Gauss-Markov stochastic processes on each subcarrier. However, as already noted in Sec. II-D, the true distribution of the S-D CFR is indeed Gaussian, while the true distribution of the composite S-R$_1$-D and S-R$_2$-D CFRs is in fact double Gaussian. Thus, the state-space model introduced in this section is a convenient approximation, which makes sense when only the first and second order moments are of interest. Our simulation results will validate this approach.

### B. Per-subcarrier S-D CFR estimation subgraph

First assume that the symbol-level probabilities $\mu_{d^n(k-1)\to g^n(k)}(d^n(k-1))$ and $\mu_{d^n(k)\to g^n(k)}(d^n(k))$ are available from (20) for all possible values of $d^n(k-1)$ and $d^n(k)$ in the $2^B$-ary alphabet, with the normalization $\sum_{d^n(k-1)} \mu_{d^n(k-1)\to g^n(k)}(d^n(k-1)) = 1$ and $\sum_{d^n(k)} \mu_{d^n(k)\to g^n(k)}(d^n(k)) = 1$. If, as per hypothesis, the continuous-valued message $\mu_{X_{\mathsf{e}}^n(k)\to g^n(k)}(X_{\mathsf{e}}^n(k))$ is Gaussian, it has the form

$$\mu_{X_{\mathsf{e}}^n(k)\to g^n(k)}(X_{\mathsf{e}}^n(k)) \propto \mathcal{N}_C(X_{\mathsf{e}}^n(k) : \hat{X}_{\mathsf{e}}^n(k\setminus k), P_{\mathsf{e}}^n(k\setminus k)), \tag{23}$$

where the smoothed S-R$_2$-D mean and variance will be given later in (30). Then, the message (8) incoming to the considered subgraph can be approximated as

$$\begin{aligned} &\mu_{g^n(k)\to X_{\mathsf{d}}^n(k)}(X_{\mathsf{d}}^n(k)) \\ &\propto \mathcal{N}_C\big(Y^n(k) : \hat{d}^n(k) X_{\mathsf{d}}^n(k) + \hat{b}_{\mathsf{e}}^n(k), S_{\mathsf{e}}^n(k)\big), \end{aligned} \tag{24}$$

where

$$\begin{aligned} \hat{d}^n(k-1) &= \sum_{d^n(k-1)} \mu_{d^n(k-1)\to g^n(k)}(d^n(k-1)) d^n(k-1) \\ \hat{d}^n(k) &= \sum_{d^n(k)} \mu_{d^n(k)\to g^n(k)}(d^n(k)) d^n(k), \end{aligned}$$

are the soft symbol estimates at the previous and current time slot. The bias term

$$\hat{b}_{\mathsf{e}}^n(k) = \hat{d}^n(k-1)\hat{X}_{\mathsf{e}}^n(k\setminus k)$$

accounts for the ISI caused by successive relaying. The variance

$$\begin{aligned} S_{\mathsf{e}}^n(k) &= R_{\mathsf{e}} \\ &+ \sum_{d^n(k-1)} \mu_{d^n(k-1)\to g^n(k)}(d^n(k-1)) \\ &\quad \times \big\{ |d^n(k-1)|^2 P_{\mathsf{e}}^n(k\setminus k) \\ &\quad + |d^n(k-1) - \hat{d}^n(k-1)|^2 |\hat{X}_{\mathsf{e}}^n(k\setminus k)|^2 \big\} \\ &+ \sum_{d^n(k)} \mu_{d^n(k)\to g^n(k)}(d^n(k)) |d^n(k) - \hat{d}^n(k)|^2 E_{\mathsf{SD}}, \end{aligned}$$

accounts for the channel noise, the residual uncertainty on the modulated data and the uncertainty on the S-D and S-R$_2$-D CFR estimates. The demonstration, based on the moment-matching method is postponed to Appendix A.

Now, we turn our attention to the forward and backward messages for S-D channel estimation on the subgraph. Assuming they are also Gaussian they can be written as

$$\begin{aligned} &\mu_{f_{\mathsf{d}}^n(k)\to X_{\mathsf{d}}^n(k)}(X_{\mathsf{d}}^n(k)) \\ &\propto \mathcal{N}_C(X_{\mathsf{d}}^n(k) : \hat{X}_{\mathsf{d}}^n(k|k-1), P_{\mathsf{d}}^n(k|k-1)) \\ &\mu_{f_{\mathsf{d}}^n(k+1)\to X_{\mathsf{d}}^n(k)}(X_{\mathsf{d}}^n(k)) \\ &\propto \mathcal{N}_C(X_{\mathsf{d}}^n(k) : \hat{X}_{\mathsf{d}}^n(k|k+1:K-1), P_{\mathsf{d}}^n(k|k+1:K-1)). \end{aligned} \tag{25}$$

Injecting the Gausian approximation (24) in the forward and backward message update equations (9)-(10), the mean and variance of the Gaussian messages in (25) are recursively updated using standard Kalman prediction and measurement update [32]. Consequently, the message (11) outgoing from the subgraph becomes

$$\mu_{X_{\mathsf{d}}^n(k)\to g^n(k)}(X_{\mathsf{d}}^n(k)) \propto \mathcal{N}_C(X_{\mathsf{d}}^n(k) : \hat{X}_{\mathsf{d}}^n(k\setminus k), P_{\mathsf{d}}^n(k\setminus k)), \tag{26}$$

where the smoothed S-D mean and variance are expressed as

$$\begin{aligned} P_{\mathsf{d}}^n(k\setminus k) &= \frac{P_{\mathsf{d}}^n(k|k-1) P_{\mathsf{d}}^n(k|k+1:K-1)}{P_{\mathsf{d}}^n(k|k-1) + P_{\mathsf{d}}^n(k|k+1:K-1)} \\ \hat{X}_{\mathsf{d}}^n(k\setminus k) &= P_{\mathsf{d}}^n(k\setminus k) \left[ \frac{\hat{X}_{\mathsf{d}}^n(k|k-1)}{P_{\mathsf{d}}^n(k|k-1)} + \frac{\hat{X}_{\mathsf{d}}^n(k|k+1:K-1)}{P_{\mathsf{d}}^n(k|k+1:K-1)} \right]. \end{aligned}$$

*Remark 4.1:* We remind that all expressions are valid for $k$ even as in Fig. 3. If $k$ is odd, the messages keep the same expression, but replacing the subscripts $\mathsf{e}$ by $\mathsf{o}$.

### C. Per-subcarrier S-R$_2$-D CFR estimation subgraph

For this subgraph, we present the messages obtained under the postulated Gaussian assumption. Demonstrations are omitted, since they follow exactly the same methodology as in Sec. IV-B.

Let us begin with the messages incoming to the subgraph. Plugging the result (26) into (12), the message $\mu_{g^n(k)\to X_{\mathsf{e}}^n(k)}(X_{\mathsf{e}}^n(k))$ is a Gaussian mixture, that we collapse to the single Gaussian

$$\begin{aligned} &\mu_{g^n(k)\to X_{\mathsf{e}}^n(k)}(X_{\mathsf{e}}^n(k)) \\ &\propto \mathcal{N}_C\big(Y^n(k) : \hat{d}^n(k-1) X_{\mathsf{e}}^n(k) + \hat{b}_{\mathsf{d}}^n(k), S_{\mathsf{d}}^n(k)\big), \end{aligned} \tag{27}$$

where the bias term

$$\hat{b}_{\mathsf{d}}^n(k) = \hat{d}^n(k)\hat{X}_{\mathsf{d}}^n(k\setminus k)$$

accounts for the source symbol contribution sent during the current time slot and the variance

$$\begin{aligned} S^n_{\mathsf{d}}(k) &= R_{\mathsf{e}} \\ &+ \sum_{d^n(k)} \mu_{d^n(k)\to g^n(k)}(d^n(k)) \\ &\quad \times \left\{ |d^n(k)|^2 P^n_{\mathsf{d}}(k \setminus k) \right. \\ &\quad \left. + |d^n(k) - \hat{d}^n(k)|^2 |\hat{X}^n_{\mathsf{d}}(k \setminus k)|^2 \right\} \\ &+ \sum_{d^n(k-1)} \mu_{d^n(k-1)\to g^n(k)}(d^n(k-1)) \\ &\quad \times |d^n(k-1) - \hat{d}^n(k-1)|^2 E_{\mathsf{SR}_2} \beta^2_{\mathsf{R}_2} \end{aligned}$$

accounts for the channel noise, the residual uncertainty on the modulated data and the uncertainty on the S-D and S-$\mathsf{R}_2$-D CFR estimates.

The message in the forward direction on the subgraph has the form

$$\begin{aligned} &\mu_{f^n_{\mathsf{e}}(k)\to X^n_{\mathsf{e}}(k)}(X^n_{\mathsf{e}}(k)) \\ &\quad \propto \mathcal{N}_C(X^n_{\mathsf{e}}(k) : \hat{X}^n_{\mathsf{e}}(k|k-1), P^n_{\mathsf{e}}(k|k-1)). \end{aligned} \tag{28}$$

During even time slots, plugging (27) into (13), the forward update rule reduces to Kalman correction followed by Kalman prediction, while during odd time slots (14) boils down to a Kalman predictor [32]. Similarly, the message in the backward direction on the subgraph has the form

$$\begin{aligned} &\mu_{f^n_{\mathsf{e}}(k+1)\to X^n_{\mathsf{e}}(k)}(X^n_{\mathsf{e}}(k)) \\ &\quad \propto \mathcal{N}_C(X^n_{\mathsf{e}}(k) : \hat{X}^n_{\mathsf{e}}(k|k+1:K), P^n_{\mathsf{e}}(k|k+1:K)). \end{aligned} \tag{29}$$

During even time slots plugging (27) into (15), the update rule reduces to Kalman correction followed by Kalman prediction, while during odd time slots (16) boils down to a Kalman predictor [32]. Consequently, the message (17) outgoing from the subgraph becomes

$$\begin{aligned} &\mu_{X^n_{\mathsf{e}}(k)\to g^n(k)}(X^n_{\mathsf{e}}(k)) \\ &\quad \propto \mathcal{N}_C(X^n_{\mathsf{e}}(k) : \hat{X}^n_{\mathsf{e}}(k \setminus k), P^n_{\mathsf{e}}(k \setminus k)), \end{aligned} \tag{30}$$

where the smoothed S-$\mathsf{R}_2$-D mean and variance are expressed as

$$\begin{aligned} P^n_{\mathsf{e}}(k \setminus k) &= \frac{P^n_{\mathsf{e}}(k|k-1) P^n_{\mathsf{e}}(k|k+1:K)}{P^n_{\mathsf{e}}(k|k-1) + P^n_{\mathsf{e}}(k|k+1:K)} \\ \hat{X}^n_{\mathsf{e}}(k \setminus k) &= P^n_{\mathsf{e}}(k \setminus k) \left[ \frac{\hat{X}^n_{\mathsf{e}}(k|k-1)}{P^n_{\mathsf{e}}(k|k-1)} + \frac{\hat{X}^n_{\mathsf{e}}(k|k+1:K)}{P^n_{\mathsf{e}}(k|k+1:K)} \right]. \end{aligned}$$

### D. Per-subcarrier S-$\mathsf{R}_1$-D CFR estimation subgraph

All messages have similar expressions to those found in Sec. IV-C, since message-passing is performed on a subgraph having the same structure. Therefore, it suffices to summarize the three steps of Gaussian message derivation. First, the messages at the input of the subgraph are collapsed to Gaussian conditional likelihoods. Secondly, depending on the slot index, the Gaussian message update rule on the subgraph in both directions has either the form of a Kalman prediction and correction, or of a Kalman prediction alone. Thirdly, outgoing messages from the subgraph are Gaussian as well, with mean and variance obtained by smoothing equations.

### E. Per-subcarrier detection subgraph

Injecting (26) and (30) into (18), the forward recursion on the detection subgraph is

$$\begin{aligned} &\mu_{g^n(k)\to d^n(k)}(d^n(k)) \\ &\propto \sum_{d^n(k-1)} \mu_{g^n(k-1)\to d^n(k-1)}(d^n(k-1)) \\ &\quad \times \mu_{m^n(k-1)\to d^n(k-1)}(d^n(k-1)) \\ &\quad \times \int\int \mathcal{N}_C\left(Y^n(k) : d^n(k) X^n_{\mathsf{d}}(k) + d^n(k-1) X^n_{\mathsf{e}}(k), R_{\mathsf{e}}\right) \\ &\qquad \times \mathcal{N}_C(X^n_{\mathsf{d}}(k) : \hat{X}^n_{\mathsf{d}}(k \setminus k), P^n_{\mathsf{d}}(k \setminus k)) \\ &\qquad \times \mathcal{N}_C(X^n_{\mathsf{e}}(k) : \hat{X}^n_{\mathsf{e}}(k \setminus k), P^n_{\mathsf{e}}(k \setminus k)) dX^n_{\mathsf{d}}(k) dX^n_{\mathsf{e}}(k), \end{aligned} \tag{31}$$

which admits an analytical expression in the form of a Gaussian mixture (see [33, p. 38])

$$\begin{aligned} &\mu_{g^n(k)\to d^n(k)}(d^n(k)) \\ &\propto \sum_{d^n(k-1)} \mu_{g^n(k-1)\to d^n(k-1)}(d^n(k-1)) \\ &\quad \times \mu_{m^n(k-1)\to d^n(k-1)}(d^n(k-1)) \\ &\times \mathcal{N}_C\Big(Y^n(k) : d^n(k) \hat{X}^n_{\mathsf{d}}(k \setminus k) + d^n(k-1) \hat{X}^n_{\mathsf{e}}(k \setminus k), \\ &\qquad |d^n(k)|^2 P^n_{\mathsf{d}}(k \setminus k) + |d^n(k-1)|^2 P^n_{\mathsf{e}}(k \setminus k) + R_{\mathsf{e}}\Big). \end{aligned} \tag{32}$$

In the same way, it is easily shown that the backward recursion (19) on the detection subgraph follows

$$\begin{aligned} &\mu_{g^n(k+1)\to d^n(k)}(d^n(k)) \\ &\quad \propto \sum_{d^n(k+1)} \mu_{g^n(k+2)\to d^n(k+1)}(d^n(k+1)) \\ &\quad \times \mu_{m^n(k+1)\to d^n(k+1)}(d^n(k+1)) \\ &\quad \times \mathcal{N}_C\big(Y^n(k+1) : d^n(k+1) \hat{X}^n_{\mathsf{d}}(k+1 \setminus k+1) \\ &\qquad + d^n(k) \hat{X}^n_{\mathsf{o}}(k+1 \setminus k+1), \\ &\qquad |d^n(k+1)|^2 P^n_{\mathsf{d}}(k+1 \setminus k+1) \\ &\qquad + |d^n(k)|^2 P^n_{\mathsf{o}}(k+1 \setminus k+1) + R_{\mathsf{o}}\big). \end{aligned} \tag{33}$$

Finally, for each symbol in the $2^B$-ary alphabet, the outgoing messages towards the demodulation subgraph is obtained as the product of the forward and backward messages as in (21).

Note that the expression of the symbol-level probabilities (20) is unaffected by the Gaussian approximation.

*Remark 4.2:* We remind that all expressions are valid for $k$ even as in Fig. 3. If $k$ is odd, the messages keep the same expression, but swapping the subscripts e and o.

### F. Demodulation and decoding subgraph

The method described in Sec. III-E implements exact message-passing on the demodulation and decoding subgraphs, so that no modification is needed here.

### G. Message-passing schedule

The presence of cycles in the factor graph of Fig. 3 gives rise to an iterative message-passing receiver. In each iteration, the following steps are carried out

1) per-subcarrier S-D CFR estimation is performed in parallel for all subcarriers, based on observations from all OFDM blocks in a frame (see Sec. IV-B). Then, per-subcarrier S-$R_2$-D CFR estimation (see Sec. IV-C) takes place, in parallel with per-subcarrier S-$R_1$-D CFR estimation (see Sec. IV-D). The computational complexity per transmitted complex symbol is $\mathcal{O}(2^B)$ for this step.
2) soft symbol detection is performed in parallel for all subcarriers, according to the forward-backward procedure described in Sec. IV-E. The computational complexity per transmitted complex symbol is $\mathcal{O}((2^B)^2)$ for this step.
3) demodulation and decoding of a frame is performed accross all subcarriers (see Sec. IV-F). Under the assumption that the bits associated with a given symbol are independent, which is justified by the presence of bit-interleaving at the transmitter, the extrinsic symbol probabilities of the form $\mu_{m^n(k)\to d^n(k)}(d^n(k))$, for $k = 0,\ldots,K-1$ and $n = 0,\ldots,N-1$, can be computed as products of extrinsic probabilities of the corresponding coded bits. The computational complexity for this step depends on the FEC scheme.

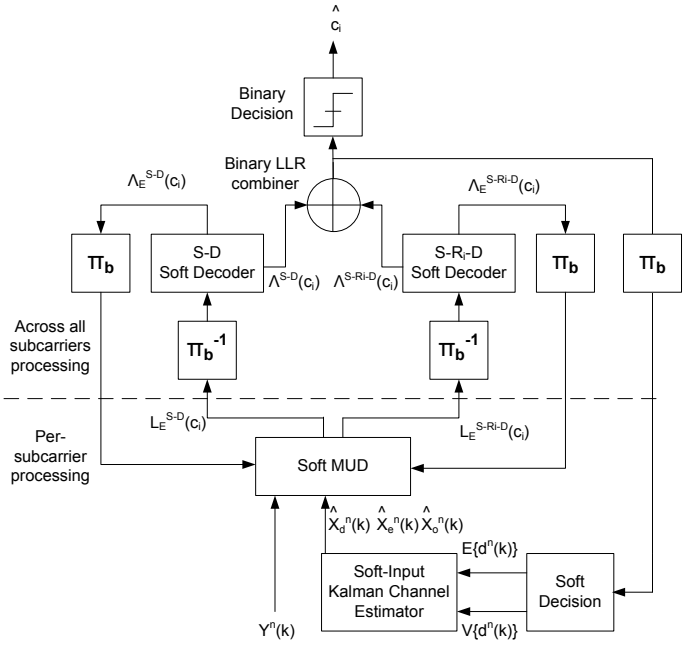


Fig. 5. Iterative multiuser detection receiver with soft-input Kalman channel estimation.

### H. Message-passing initialization

At the first iteration, a suitable initialization is needed for the symbol-level probabilities (20). In the absence of prior knowledge, all those messages are initialized to the uniform probability mass function. Similarly at the first iteration, the messages $\mu_{X_{\mathsf{e}}^n(k)\to g^n(k)}(X_{\mathsf{e}}^n(k))$ for even time slot indices $k$ (resp. $\mu_{X_{\mathsf{o}}^n(k)\to g^n(k)}(X_{\mathsf{o}}^n(k))$ for odd time slot indices $k$) need to be initialized as Gaussians whose mean and variance are chosen as their prior values given by (5).

Furthermore, irrespective of the iteration index, the forward and backward CFR estimation messages for each subcarrier need proper pilot-based initialization for the first and last time slot, in order to bootstrap the proposed receiver. Here we assume that frequency interleaving is not used for pilot OFDM blocks. For each frame, during the three pilot OFDM blocks at the beginning of the current frame (see Fig. 1), the S-D, S-$R_2$-D, S-$R_1$-D CFR's frequency correlation can be modeled with a Gauss-Markov process, so that data-aided Kalman smoothing [34] can be used to initialize the mean and variance of the forward CFR estimation messages for each subcarrier for the first time slot. In the same way, the three OFDM pilot blocks at the beginning of the next frame are used to initialize the backward CFR estimation messages for each subcarrier for the last time slot.

### I. Comparison with existing message-passing methods

We seek a benchmark algorithm with more or less the same computational complexity than the proposed method, taken from the class of multiuser detectors and adapted to the observation model of Sec. II-D and the CFR state-space model of Sec. IV-A. The resulting iterative method, depicted in Fig. 5, performs both per-subcarrier and across all subcarriers processing. On the $n$-th subcarrier, coupled estimation of S-D, S-$R_1$-D and S-$R_2$-D CFRs uses a soft-input Kalman smoother [35], fed with the expectation and variance of symbols $\{d^n(k)\}_{k=0}^{K-1}$. Based on these channel estimates, the maximum *a posteriori* (MAP) multiuser detector (MUD) developed in [36] delivers extrinsic log-likelihood ratios (LLR) on the coded bits for the direct path (denoted by $L_E^{\mathsf{S-D}}$) and the relay path (denoted by $L_E^{\mathsf{S-R_i-D}}$), which interfere at the destination. Soft decoding, performed across all subcarriers, delivers both *a posteriori* and extrinsic LLRs on the coded bits, by taking the code constraints into account [36]. *A posteriori* and extrinsic LLRs on the direct path are denoted by $\Lambda^{\mathsf{S-D}}$ and $\Lambda_E^{\mathsf{S-D}}$, respectively. Similarly, *a posteriori* and extrinsic LLRs on the relay path are denoted by $\Lambda^{\mathsf{S-R_i-D}}$ and $\Lambda_E^{\mathsf{S-R_i-D}}$, respectively. Extrinsic LLRs at the decoder output are fed back as *a priori* information to the MAP MUD. *A posteriori* LLRs at the decoder outputs are fed to a LLR combiner (adder) before hard decison, in order to extract the spatial diversity (the rationale behind this operation is that coded bits decoded on the direct and relay paths stem from the same source message). Moreover, the combined LLRs are fed back to a soft decision device computing the expectation and variance of the complex symbols for the purpose of channel re-estimation. Note that, the benchmark method uses the CFR estimates as if they were the true values. Thus unlike the proposed method, potentially important CFR reliability information is discarded.

## V. Simulation results

We now present simulation results to evaluate the performances of the proposed amplify-and-forward successive relaying (AF-SR) scheme with imperfect and time-varying CSI. Our AF-SR low-complexity receiver of Sec. IV is compared to

1) the AF-SR perfect CSI receiver: the proposed method with perfect knowledge of all CFRs, which boils down

to a turbo-equalizer on the equivalent memory-1 ISI channel
2) the AF-SR classical pilot-only receiver: the proposed method with CFR estimation message-passing enabled only at the first iteration, which boils down to a turbo-equalizer with CFR temporal interpolation between two consecutive pilot blocks based on Kalman smoothing.
3) the AF-SR iterative MUD benchmark receiver of Sec. IV-I.

For the sake of completeness, we also present results for the direct-only low-complexity receiver, which is the proposed method of Sec. IV in the non-cooperative case (i.e. only the direct S-D link exists, while $\mathsf{R}_1$ and $\mathsf{R}_2$ always remain silent) with imperfect and time-varying CSI.

### A. Simulation parameters

$\mathsf{S}$ implements bit-interleaved coded modulation using a rate-$1/2$ FEC code which is

- either the de facto standard memory-6 convolutional code (CC) with generators $(171, 131)$ in octal [37].
- or a $(3, 6)$ regular low-density parity-check (LDPC) code [22].

The mapper's modulation type is either binary phase shift keying (BPSK), Gray-coded quadrature phase shift keying (QPSK) or 8-ary phase shift keying (8-PSK). Referring to Fig. 1, the modulated symbols at $\mathsf{S}$ are arranged in frames containing $K = 14$ data OFDM modulated blocks, preceded by three pilot blocks, with $N = 256$ subcarriers and a CP of length $G = N/8$. A pseudo-random bit-interleaver $\pi_b(.)$ (resp. frequency interleaver $\pi_f(.)$) acts on each frame (resp. on the subcarriers of each OFDM symbol).

The CIR between any two nodes $\mathsf{A}$ and $\mathsf{B}$ $\{h^l_{\mathsf{A},\mathsf{B}}(k)\}_{l=0}^{L-1}$ is assumed to have a finite length $L = N/16$, so that the CP is long enough to prevent IBI, and a normalized power delay profile (PDP) given by

$$E[|h^l_{\mathsf{A},\mathsf{B}}(k)|^2] = \frac{1-e^{-3}}{1-e^{-3L}} e^{-3l},\ l = 0, \ldots, L-1.$$

All CIRs are independent with block fading time-variations following the Jakes' Doppler power spectrum, simulated with the method described in [38]. Assume that $\mathsf{R}_1$ and $\mathsf{R}_2$ are fixed and that $\mathsf{S}$ and $\mathsf{D}$ are moving. Let $B_d$ denote the maximum Doppler shift (in Hertz) at $\mathsf{S}$, $\mathsf{D}$ and let $T$ denote the duration of an OFDM block (in seconds), then the temporal autocorrelation of the channel taps is given by

$$E[h^l_{\mathsf{A},\mathsf{B}}(k) h^l_{\mathsf{A},\mathsf{B}}(k-m)^*] = J_0(2\pi m B_d T),\ l = 0, \ldots, L-1$$

where $J_0$ is the zero-order Bessel function of first kind. We retain two block fading scenarios:

- either slow fading, with a normalized fading rate $B_d T_s = 5 \times 10^{-6}$
- or fast fading, with a normalized fading rate $B_d T_s = 5 \times 10^{-5}$,

where $T_s = T/(N+G)$ denotes the sampling period. We also consider a realistic scenario, where $\mathsf{R}_1$ and $\mathsf{R}_2$ are located between $\mathsf{S}$ and $\mathsf{D}$, so that the average $\mathsf{S}-\mathsf{D}$ channel quality is worse than the $\mathsf{S}-\mathsf{R}_1$ and $\mathsf{S}-\mathsf{R}_2$ channel quality. In our simulations, $E_{\mathsf{SR}_1}/E_{\mathsf{SD}} = E_{\mathsf{SR}_2}/E_{\mathsf{SD}} = 4$ dB. Furthermore, in order to relax the power supply constraints at $\mathsf{R}_1$ and $\mathsf{R}_2$, we assume equal power reception at $\mathsf{D}$, so that $E_{\mathsf{R}_1\mathsf{D}}/E_{\mathsf{SD}} = E_{\mathsf{R}_2\mathsf{D}}/E_{\mathsf{SD}} = 0$ dB. It follows that the signal-to-noise ratio (SNR) of the direct path $E_{\mathsf{SD}}/N_0$ is a sufficient parameter for performance evaluation. We list here the sources of power efficiency loss:

- a power efficiency loss with a factor of $N/(N+G)$ due to CP insertion
- a power efficiency loss with a factor of $(K+1)/(K+4)$ due to pilot insertion.

The receiver at $\mathsf{D}$ assumes CFR temporal dynamics given by (22). From an implementation point of view, it makes more engineering sense to keep the driving noise variances $q_{\mathsf{d}}$, $q_{\mathsf{e}}$ and $q_{\mathsf{o}}$ at constant values, instead of having to estimate them as hyperparameters depending on the channel time-selectivity. Therefore, we set $q_{\mathsf{d}} = q_{\mathsf{e}} = q_{\mathsf{o}} = 0.4$, as our simulations showed that these values can accomodate both slow and fast fading scenarios.

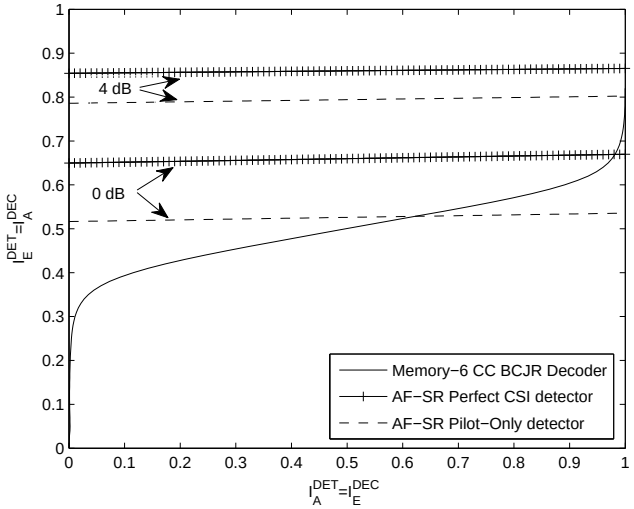


Fig. 6. EXIT chart for the AF-SR perfect CSI detector and AF-SR classical pilot-aided detector, parameterized by different values of $E_{\mathsf{SD}}/N_0$ in slow fading conditions, i.e. $B_{\mathsf{d}} T_s = 5 \times 10^{-6}$.

### B. Influence of the fading rate

*1) EXIT analysis:* The proposed AF-SR low-complexity receiver is not directly amenable to an EXIT analysis [39], since CFR estimation at a given iteration is not independent of CFR accurracy at the previous iteration (see (24) for instance). However, we present EXIT charts for

1) the AF-SR perfect CSI detector
2) and the AF-SR classical pilot-aided detector

in order to evaluate the potential for performance improvement using the proposed AF-SR low-complexity receiver, under different fading conditions.

Here, we use BPSK modulation and memory-6 convolutional encoding with slow or fast fading. Let $I_A^{DET}$ denote the mutual information (MI) between the encoded bits and the *a priori* log-likelihood ratios (LLRs) at the AF-SR perfect CSI

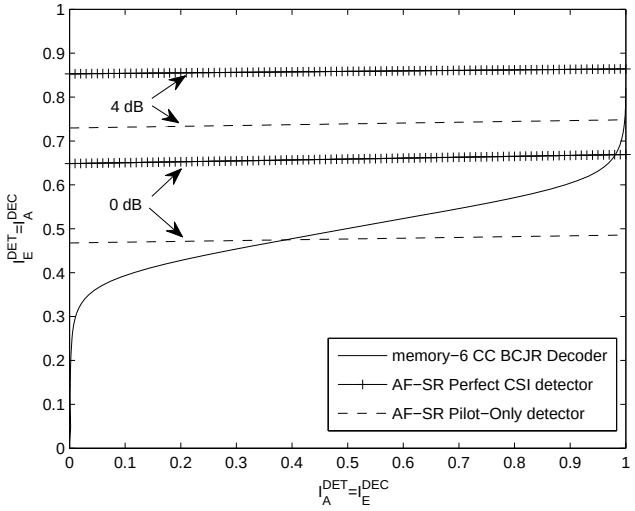


Fig. 7. EXIT chart for the AF-SR perfect CSI detector and AF-SR classical pilot-aided detector, parameterized by different values of $E_{\mathsf{SD}}/N_0$ in fast fading conditions, i.e. $B_{\mathsf{d}}T_s = 5 \times 10^{-5}$.

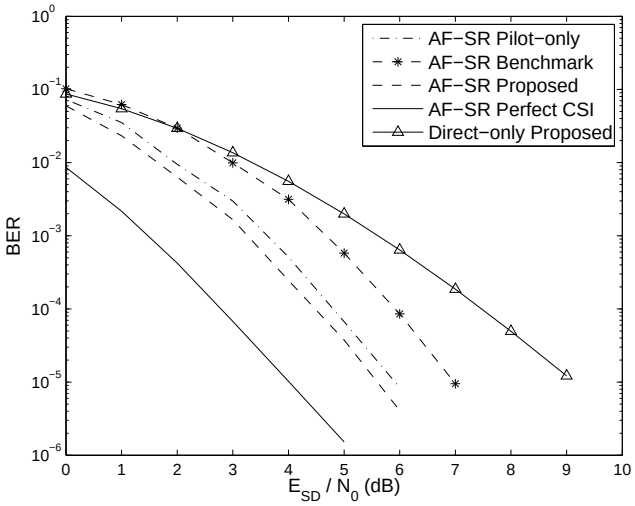


Fig. 8. BER using the memory-6 CC and BPSK under slow fading after 2 iterations: comparison of the AF-SR pilot-only (dash dotted), benchmark iterative MUD (star), proposed (dashed) and perfect CSI (solid) methods with non-cooperative direct $\mathsf{S}-\mathsf{D}$ link-only reception (triangles).

or AF-SR classical pilot-aided detector input [39]. Similarly, let $I_E^{DET}$ denote the MI between the encoded bits and the *extrinsic* LLRs at the AF-SR perfect CSI or AF-SR classical pilot-aided detector output [39]. Assuming sufficient bit interleaving, the corresponding transfer characteristic, denoted by

$$I_E^{DET} = T^{DET}(I_A^{DET}, E_{\mathsf{SD}}/N_0)$$

can be obtained by Monte Carlo simulations, assuming that all *a priori* LLRs are i.i.d. distributed according to a symmetric Gaussian [39]. Furthermore, let $I_A^{DEC}$ (resp. $I_E^{DEC}$) denote the MI between the encoded bits and the *a priori* LLRs at the BCJR decoder input (resp. the MI between the encoded bits and the *extrinsic* LLRs at the BCJR decoder output), the transfer characteristic,

$$I_E^{DEC} = T^{DEC}(I_A^{DEC})$$

is obtained in the same way.

Fig. 6 (resp. Fig. 7) illustrates the EXIT chart in the slow (resp. fast) fading scenario. The receiver performance after convergence is determined by the intersection of the EXIT curves corresponding to the detector and the FEC decoder [39]. At high SNR (here $E_{\mathsf{SD}}/N_0 = 4$ dB) and using the perfect CSI receiver, those intersections almost coincide for slow and fast fading. However, regarding the pilot-only receiver, the performance gap with respect to (wrt) perfect CSI is much larger for fast fading than for slow fading. This indicates that, when replacing the pilot-only receiver by the proposed low-complexity receiver, there is more room for performance improvement in the fast fading than in the slow fading scenario.

*2) BER performance:* Fig. 8 (resp. Fig. 9) compares the bit-error rate (BER) for the AF-SR proposed low-complexity receiver with the BER of the perfect CSI, pilot-only and benchmark receivers, in the slow (resp. fast) fading scenario. The non-cooperative BER curve (i.e. when only the direct $\mathsf{S}-\mathsf{D}$ path exists) using the proposed low-complexity receiver

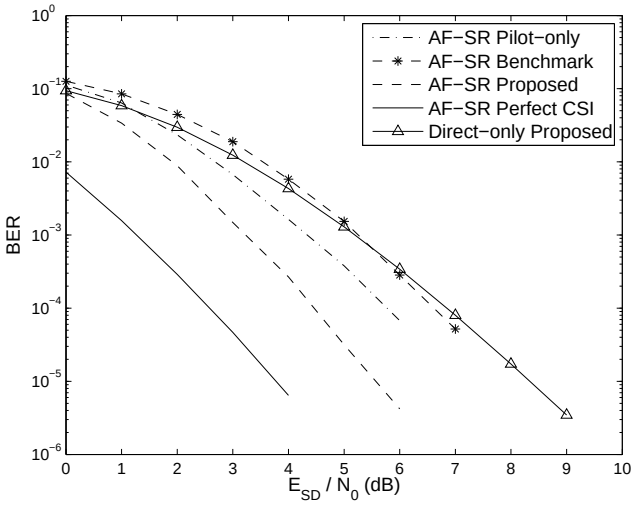


Fig. 9. BER using the memory-6 CC and BPSK under fast fading after 2 iterations: comparison of the AF-SR pilot-only (dash dotted), benchmark iterative MUD (star), proposed (dashed) and perfect CSI (solid) methods with non-cooperative direct $\mathsf{S}-\mathsf{D}$ link-only reception (triangles).

is also shown for reference. All receivers use two iterations, since no BER improvement was obtained by further increasing the number of iterations. Not surprisingly, the BER of the proposed receiver coincides with (resp. outperforms) the BER of the pilot-only receiver at iteration 1 (resp. at iteration 2). In particular, increasing the iteration index from 1 to 2 in the fast fading scenario, a BER improvement of one order of magnitude at $E_{\mathsf{SD}}/N_0 = 6$ dB is obtained. We observe that the spatial diversity order of the non-cooperative scheme is 1, while the AF-SR scheme benefits from a diversity order of 2, thanks to the transmit diversity induced by successive relaying [4]-[5]. As expected from the EXIT analysis in Sec. V-B1, the BERs of the AF-SR perfect CSI receiver

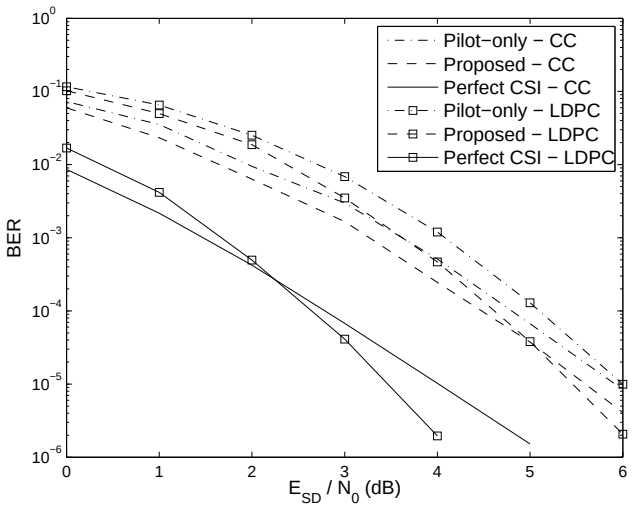


Fig. 10. BER using BPSK under slow fading, for the AF-SR proposed, pilot-only and perfect CSI methods with a memory-6 CC (after 2 iterations) or a $(3584, 3, 6)$ regular LDPC code (after 4 iterations).

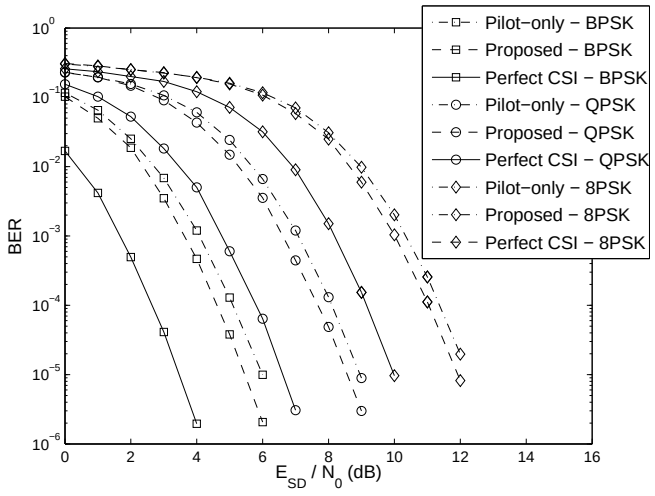


Fig. 11. BER using a $(3584, 6)$ regular LDPC code for BPSK/ $(7168, 6)$ regular LDPC code for QPSK/ $(10752, 6)$ regular LDPC code for 8-PSK under slow fading, for the AF-SR proposed, pilot-only and perfect CSI methods after 4 iterations.

under the slow and fast fading scenario are comparable at $E_{\mathsf{SD}}/N_0 = 4$ dB. Also, the proposed AF-SR low-complexity receiver is 0.3 dB (resp. 1.3 dB) more power efficient than the pilot-only receiver at a BER of $10^{-4}$, under the slow (resp. fast) fading scenario. We interpret these results by the fact that the pilot-only receiver's Kalman-based CFR temporal interpolation between two successive pilot blocks performs well under slow fading. However under fast fading, the AF-SR pilot-only receiver induces large CFR estimation errors, that substantially erode the achievable diversity gain. By exploiting *a priori* information on the data symbols between the pilot blocks, the proposed low-complexity receiver can better reconstruct the CFRs and gain back the diversity loss.

The performance gap between the AF-SR proposed low-complexity receiver and the perfect CSI receiver can be interpreted as the combined effect of residual CFR estimation uncertainty due to detrimental noise amplification at the relays and the Gaussian approximation needed to get a tractable message-passing algorithm.

Also note that the benchmark iterative MUD with soft-input Kalman CFR estimation has the worst performances among all iterative AF-SR receivers, both under slow and fast fading. Indeed, the first disadvantage of the benchmark method is that it lacks the possibility of exploiting CFR reliability information. More importantly, iterative MUD works best under the assumptions of independence and sufficient bit-interlaving between the detected data streams. Those conditions are obviously not met since the data streams to be detected correspond to the S-D and S-R$_i$-D paths, which not only stem from the same source message, but are also only one time slot apart.

### C. Influence of the FEC code

Here, we study the sensitivity of the proposed receiver to FEC on our OFDM AF-SR channel, which is equivalent to a memory-1 ISI block fading channel.

If the memory-6 CC is used, at each receiver iteration, one round of BCJR decoding [14] is performed, which implements exact message-passing on the decoding subgraph in Fig. 3.

When the $(3, 6)$ regular LDPC code is employed, belief-propagation decoding [22] is used. This decoder also implements message-passing, but since the decoding subgraph is loopy, several iterations are needed in order to obtain soft decisions on the coded bits, that are sufficiently reliable. Our experiments showed that performing 5 rounds of belief-propagation decoding at each receiver iteration leads to satisfactory results.

Fig. 10 compares the simulation results for the rate-$1/2$ memory-6 CC and the $(3584, 3, 6)$ regular LDPC code. The AF-SR scheme with BPSK signalling in the slow fading scenario is considered. Furthermore, it was found that all iterative receivers needs two rounds using CC (resp. four rounds using LDPC) in order to reach convergence. At low SNR, the performances of all receivers are worse for the LDPC than for the CC FEC scheme. Conversely, for sufficiently high SNRs, the performances of all receivers will eventually be better for the LDPC than for the CC FEC scheme. Indeed for a fixed coding rate, it is well-known that LDPC codes typically achieve lower error rates than convolutional codes at medium to high SNR values [41]. Comparable results (although not shown here) were obtained in the fast fading scenario.

### D. Influence of the modulation format

We now consider the AF-SR system, with rate-$1/2$ $(3, 6)$ regular LDPC encoding for three types of modulation, that is BPSK, Gray-coded QPSK and Gray-coded 8-PSK. Fig. 11 illustrates the BER of all considered receivers after 4 iterations, in the slow fading scenario. Note the difference in terms of symbol energy to noise power spectral density between BPSK and Gray-coded QPSK is 3 dB, as expected [25]. Also, the SNR gain of the proposed low-complexity receiver wrt the classical pilot-based approach is 0.5 dB (resp. 0.3 dB) at a

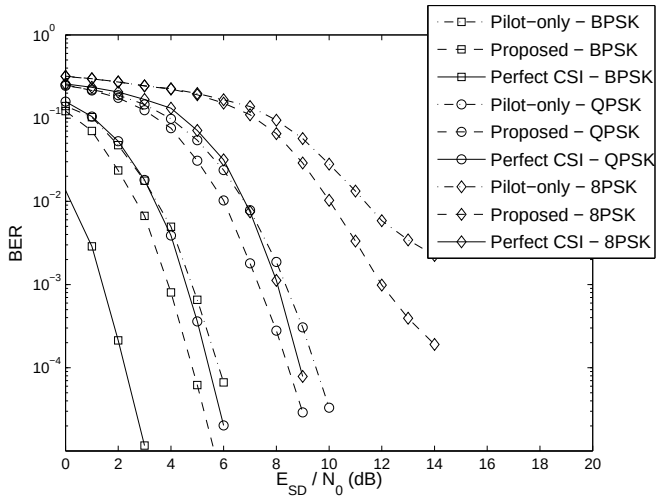


Fig. 12. BER using a $(3584, 6)$ regular LDPC code for BPSK/ $(7168, 6)$ regular LDPC code for QPSK/ $(10752, 6)$ regular LDPC code for 8-PSK under fast fading, for the AF-SR proposed, pilot-only and perfect CSI methods after $4$ iterations.

BER of $10^{-4}$ for BPSK and QPSK (resp. 8-PSK). Similar results in Fig. 12 for the fast fading scenario, show that the SNR gain of the proposed low-complexity receiver wrt the classical pilot-based approach is even more pronounced.

## VI. Conclusion

In this paper, we introduced a message-passing algorithm suitable for joint channel estimation, symbol detection and decoding for OFDM-based amplify-and-forward successive relaying (AF-SR) protocols. Numerical simulations showed that the resulting algorithm outperforms classical pilot-based and multiuser detectors, especially for rapid temporal channel variations. This behavior is mainly due to the code-aided nature of the proposed method, which enables iterative channel reconstruction, using soft information from the decoder.

In future work, we will focus on several extensions of the present work. In the absence of frequency interleaving, a straightforward generalization would use explicit modeling of the channel frequency correlation, by processing a chunk of contiguous subcarriers, but at the cost of a significant complexity increase. Moreover, instead of Gaussian processes it would be worthwhile to look for other models, that better match the true distribution of the channel frequency responses, while keeping a tractable formulation for message-passing. Finally, the design of near capacity-achieving codes for AF-SR protocols in the spirit of reference [42], is yet another open problem.

## Appendix A

From (23), the conditional likelihood (8) can be expressed as

$$\begin{aligned}
&\mu_{g^n(k)\to X_{\mathsf{d}}^n(k)}(X_{\mathsf{d}}^n(k)) \\
&\propto \sum_{d^n(k-1)} \sum_{d^n(k)} \mu_{d^n(k-1)\to g^n(k)}(d^n(k-1)) \\
&\quad \times \mu_{d^n(k)\to g^n(k)}(d^n(k)) \\
&\quad \times \int \mathcal{N}_C(Y^n(k) : X_{\mathsf{d}}^n(k)d^n(k) + X_{\mathsf{e}}^n(k)d^n(k-1), R_{\mathsf{e}}) \\
&\qquad \times \mathcal{N}_C(X_{\mathsf{e}}^n(k) : \hat{X}_{\mathsf{e}}^n(k \setminus k), P_{\mathsf{e}}^n(k \setminus k))dX_{\mathsf{e}}^n(k).
\end{aligned}$$

Since each integral in the above summation has the form of a Kalman correction step, we obtain the following Gaussian mixture

$$\begin{aligned}
&\mu_{g^n(k)\to X_{\mathsf{d}}^n(k)}(X_{\mathsf{d}}^n(k)) \\
&\propto \sum_{d^n(k-1)} \sum_{d^n(k)} \mu_{d^n(k-1)\to g^n(k)}(d^n(k-1)) \\
&\quad \times \mu_{d^n(k)\to g^n(k)}(d^n(k)) \\
&\quad \times \mathcal{N}_C\Big(Y^n(k) : X_{\mathsf{d}}^n(k)d^n(k) + \hat{X}_{\mathsf{e}}^n(k \setminus k)d^n(k-1), \\
&\qquad\qquad |d^n(k-1)|^2 P_{\mathsf{e}}^n(k \setminus k) + R_{\mathsf{e}}\Big),
\end{aligned}$$

that we wish to collapse to a single Gaussian with mean $m(X_{\mathsf{d}}^n(k))$ and variance $S(X_{\mathsf{d}}^n(k))$. Using moment-matching [33, p. 107] the mean is obtained as

$$\begin{aligned}
&m(X_{\mathsf{d}}^n(k)) \\
&= \sum_{d^n(k-1)} \sum_{d^n(k)} \mu_{d^n(k-1)\to g^n(k)}(d^n(k-1))\mu_{d^n(k)\to g^n(k)}(d^n(k)) \\
&\qquad\qquad \times \Big(X_{\mathsf{d}}^n(k)d^n(k) + \hat{X}_{\mathsf{e}}^n(k \setminus k)d^n(k-1)\Big) \\
&= \left(\sum_{d^n(k-1)} \mu_{d^n(k-1)\to g^n(k)}(d^n(k-1))\right) \\
&\quad \times \left(\sum_{d^n(k)} \mu_{d^n(k)\to g^n(k)}(d^n(k))d^n(k)X_{\mathsf{d}}^n(k)\right) \\
&+ \left(\sum_{d^n(k)} \mu_{d^n(k)\to g^n(k)}(d^n(k))\right) \\
&\quad \times \left(\sum_{d^n(k-1)} \mu_{d^n(k-1)\to g^n(k)}(d^n(k-1))d^n(k-1)\hat{X}_{\mathsf{e}}^n(k \setminus k)\right).
\end{aligned}$$

Assuming that the proper normalization of the symbol-level probabilities in Sec. IV-B hold, (i.e. $\sum_{d^n(k-1)} \mu_{d^n(k-1)\to g^n(k)}(d^n(k-1)) = 1$ and $\sum_{d^n(k)} \mu_{d^n(k)\to g^n(k)}(d^n(k)) = 1$), we have

$$m(X_{\mathsf{d}}^n(k)) = \hat{d}^n(k)X_{\mathsf{d}}^n(k) + \hat{d}^n(k-1)\hat{X}_{\mathsf{e}}^n(k \setminus k),$$

which is the desired result in (24). Similarly, according to the moment-matching method the desired variance is obtained as

$$\begin{aligned}
&S(X_{\mathsf{d}}^n(k))\\
&= \sum_{d^n(k-1)} \sum_{d^n(k)} \mu_{d^n(k-1)\to g^n(k)}(d^n(k-1))\mu_{d^n(k)\to g^n(k)}(d^n(k))\\
&\times \Big[|d^n(k-1)|^2 P_{\mathsf{e}}^n(k\setminus k) + R_{\mathsf{e}}\\
&\quad + \Big(X_{\mathsf{d}}^n(k)d^n(k) + \hat{X}_{\mathsf{e}}^n(k\setminus k)d^n(k-1) - m(X_{\mathsf{d}}^n(k))\Big)\\
&\quad \times \Big(X_{\mathsf{d}}^n(k)d^n(k) + \hat{X}_{\mathsf{e}}^n(k\setminus k)d^n(k-1) - m(X_{\mathsf{d}}^n(k))\Big)^*\Big].
\end{aligned}$$

Injecting the value of $m(X_{\mathsf{d}}^n(k))$ into this expression leads to

$$\begin{aligned}
&S(X_{\mathsf{d}}^n(k))\\
&= R_{\mathsf{e}}\\
&+ \sum_{d^n(k-1)} \mu_{d^n(k-1)\to g^n(k)}(d^n(k-1))\\
&\quad \times \big\{|d^n(k-1)|^2 P_{\mathsf{e}}^n(k\setminus k)\\
&\qquad + |d^n(k-1) - \hat{d}^n(k-1)|^2 |\hat{X}_{\mathsf{e}}^n(k\setminus k)|^2\big\}\\
&+ \sum_{d^n(k)} \mu_{d^n(k)\to g^n(k)}(d^n(k))|d^n(k) - \hat{d}^n(k)|^2 |X_{\mathsf{d}}^n(k)|^2.
\end{aligned}$$

Finally, averaging out $X_{\mathsf{d}}^n(k)$ using (4), the expectation of $S(X_{\mathsf{d}}^n(k))$ is the desired value, $S_{\mathsf{e}}^n(k)$ in (24).

## REFERENCES


[1] J.N. Laneman, D.N.C. Tse and G.W. Wornell, "Cooperative diversity in wireless networks: Efficient protocols and outage behavior," *IEEE Trans. Information Theory*, vol. 50, no. 12, pp. 3062-3080, Dec. 2004.

[2] N. Bhushan, L. Junyi, D. Malladi, R. Gilmore, D. Brenner, A. Damnjanovic, R. Sukhavasi, C. Patel and S. Geirhofer, "Network densification: The dominant theme for wireless evolution into 5G," *IEEE Commun. Mag.*, pp. 8289, vol. 52, no. 2, Feb. 2014.

[3] Z. Ding and K.K. Leung, "Cross-layer routing using cooperative transmission in vehicular ad-hoc networks," *IEEE Journal on Selected Areas in Communications*, pp. 571-581, vol. 29, no. 3, Mar. 2011.

[4] T. Oechtering and A. Sezgin, "A new cooperative transmission scheme using the space-time delay code," *Proc. ITG Workshop on Smart Antennas*, pp. 41-48, Munich, Germany, Mar. 2004.

[5] B. Rankov and A. Wittneben, "Spectral efficient protocols for half-duplex fading relay channels," *IEEE Journal on Selected Areas in Communications*, pp. 379-389, vol. 25, no. 2, Feb. 2007.

[6] C. Zhai, W. Zhang and P.C. Ching, "Cooperative spectrum sharing based on two-path successive relaying," *IEEE Trans. Commun.*, pp. 2260-2270, vol. 61, no. 6, June 2013.

[7] D.S. Michalopoulos and G.K. Karagiannidis, "Bypassing orthogonal relaying transmissions via spatial signal separation," *IEEE Trans. Commun.*, pp. 3028-3038, vol. 58, no. 10, Oct. 2010.

[8] L. Li, L. Wang and L. Hanzo, "Successive AF/DF relaying in the cooperative DS-CDMA uplink: Capacity analysis and its system architecture", *IEEE Trans. Veh. Technol.*, pp. 655-666, vol. 62, no. 2, Feb. 2013.

[9] S.-H. Park, K.-H. Park, Y.-C. Ko and M.-S. Alouini, "Alternate transmission relaying based on interference alignment in 3-relay half-duplex MIMO systems," *IEEE Journal on Selected Areas in Communications*, pp. 1383-1389, vol. 30, no. 8, Sept. 2012.

[10] Z. Li, X.-G. Xia and B. Li, "Achieving full diversity and fast ML decoding via simple analog network coding for asynchronous two-way relay networks," *IEEE Trans. Commun.*, pp. 3672-3681, vol. 57, no. 12, Dec. 2009.

[11] H. Mostafa, M. Marey, M.H. Ahmed and O.A. Dobre, "Simplified maximum-likelihood detectors for full-rate alternate-relaying cooperative systems", *IET Commun.*, pp. 1899-1906, vol. 7, Iss. 17, 2013.

[12] J.-S. Baek and J.-S Seo, "Efficient iterative SIC and detection for two-path cooperative block transmission relaying", *IEEE Comm. Lett.*, pp. 199-201, vol. 16, no. 2, Feb. 2012.

[13] R. Zhang, "On achievable rates of two-path successive relaying," *IEEE Trans. Commun.*, pp. 2914-2917, vol. 57, no. 10, Oct. 2009.

[14] L.R. Bahl, J. Cocke, F. Jelinek and J. Raviv, "Optimal decoding of linear codes for minimizing symbol error rate," *IEEE Trans. Inform. Theory*, Vol. 20, pp. 284-287, March 1974.

[15] H. Mostafa, M. Marey, M.H. Ahmed and O.A. Dobre, "Decoding techniques for alternate-relaying BICM cooperative systems," *EURASIP J. Wireless Comm. Netw.*, pp. 1-13, 2013.

[16] A.S. Lalos, A.A. Rontogiannis and K. Berberidis, "Frequency domain channel estimation for cooperative communication networks," *IEEE Trans. Sig. Proc.*, pp. 3400-3405, vol. 58, no. 6, June 2010.

[17] I. Prodan, T. Obara, F. Adachi and H. Gacanin, "Performance of pilot-assisted channel estimation without feedback for broadband ANC systems using OFDM access," *EURASIP J. Wireless Comm. Netw.*, pp. 1-10, Oct. 2012.

[18] M. Zhao, Z. Shi and M.C. Reed, "Iterative turbo channel estimation for OFDM system over rapid dispersive fading channel," *IEEE Trans. Wireless Commun.*, pp. 3174-3184, vol. 7, no. 8, Aug. 2008.

[19] F. R. Kschischang, B. J. Frey and H.-A. Loeliger, "Factor graph and the sum-product algorithm ," *IEEE Trans. Information Theory*, vol. 47, no. 2, pp. 498-519, Feb. 2001.

[20] H.-A. Loeliger, "An introduction to factor graphs," *IEEE Sig. Proc. Mag.*, pp. 28-41, vol. 21, no. 1, Jan. 2004.

[21] H. Sari, G. Karam and I. Jeanclaude, "Transmission techniques for digital terrestrial TV broadcasting," *IEEE Commun. Mag.*, pp. 100-109, vol. 33, no. 2, Feb. 1995.

[22] T. Richardson and R. Urbanke, *Modern coding theory*, New-York, NY: Cambridge University Press, 2008.

[23] D.M. Malioutov, J.K. Johnson and A.S. Willsky, "Walk-sums and belief propagation in Gaussian graphical models," *The Journal of Machine Learning Research*, vol. 7, pp. 2031-2064, Oct. 2006.

[24] W.Y. Zou and Y. Wu, "COFDM: An overview," *IEEE Trans. Broadcast.*, vol. 41, no. 1, pp. 18, Mar. 1995.

[25] G.L. Stüber, *Principles of Mobile Communications.* Norwell, MA: Kluver Academic Publishers, 1999.

[26] A. Nosratinia, T.E. Hunter and A. Hedayat, "Cooperative communication in wireless networks," *IEEE Commun. Mag.*, pp. 74-80, vol. 42, no. 10, Oct. 2004.

[27] M. Morelli, "Timing and frequency synchronization for the uplink of an OFDMA system," *IEEE Trans. Commun.*, pp. 296-306, vol. 52, no. 2, Feb. 2004.

[28] N. O'Donoughue and J. M. F. Moura, "On the product of independent complex Gaussians," *IEEE Trans. Sig. Proc.*, pp. 1050-1063, vol. 60, no. 3, Mar. 2012.

[29] B.M. Kurkoski, P.H. Siegel, and J.K. Wolf, "Joint message-passing decoding of LDPC codes and partial-response channels," *IEEE Trans. Information Theory*, pp. 1410-1422, vol. 48, no. 6, June 2002.

[30] X. Li, A. Chindapol and J.A. Ritcey, "Bit-interleaved coded modulation with iterative decoding and 8-PSK signaling," *IEEE Trans. Comm*, pp. 1250-1257, vol. 50, no. 8, Aug. 2002.

[31] T. Wo, P. A. Hoeher and Z. Shi, "Graph-based soft channel estimation for fast fading channels," *IEEE Trans. Wireless Comm.*, pp. 42434251, vol. 11, no. 12, Dec. 2012.

[32] D.C. Fraser and J.E. Potter, "The optimum linear smoother as a combination of two optimum linear filters," *IEEE Trans. Automat. Contr.*, pp. 387-390, vol. 14, no. 4, Aug. 1969.

[33] H. Tanizaki, *Nonlinear filters: estimation and applications*, Berlin, Germany: Springer, 1996.

[34] G. Colavolpe, A. Barbieri, and G. Caire, "Algorithms for iterative decoding in the presence of strong phase noise," *IEEE J. Sel. Areas Commun.*,vol. 23, no. 9, pp. 17481757, Sep. 2005.

[35] S. Song, A. C. Singer and K.-M. Sung, "Soft input estimation for turbo equalization," *IEEE Trans. Sig. Proc.*, pp. 2885-2894, vol. 52, no. 10, Oct. 2004.

[36] M.C. Reed, C.B. Schlegel, P.D. Alexander and J.A. Asenstorfer, "Iterative multiuser detection for CDMA with FEC: near-single-user performance," *IEEE Trans. Commun.*, vol. 46, no. 12, pp. 1693-1699, Dec. 1998.

[37] J.A. Heller and I.M. Jacobs, "Viterbi decoding for satellite and space Communication," *IEEE Trans. on Comm. Tech.*, vol. 19, no. 5, pp. 835-848, Oct. 1971.

[38] Y. Li and X. Huang, "The simulation of independent Rayleigh faders," *IEEE Trans. Commun.*, vol. 50, no. 9, pp. 1503-1514, Sept. 2002.

[39] S. ten Brink, "Convergence behavior of iteratively decoded parallel concatenated codes," *IEEE Trans. Comm.*, vol. 49, no. 10, pp. 1727-1737, Oct. 2001.

[40] S. Hara and R. Prasad, *Multicarrier techniques for mobile 4G communications*, Norwood, MA: Artech House, 2003.
[41] K. Gracie and M.-H. Hamon, "Turbo and turbo-like codes: principles and applications in telecommunications," *IEEE Proc. of the IEEE*, vol. 95, no. 6, pp. 1228-1254, June 2007.
[42] S. ten Brink, G. Kramer and A. Ashikhmin, "Design of low-density parity-check codes for modulation and decoding," *IEEE Trans. Comm.*, vol. 52, no. 4, pp. 670-678, Apr. 2004.

**Frederic Lehmann** received the E.E. degree and the M.S.E.E. degree from ENSERG, France, in 1998. In 2002, he received the PhD in Electrical Engineering from the National Polytechnical Institute, Grenoble (INPG), France. He worked as a Research Engineer with STMicroelectronics from 1999 to 2002. From 2003 to 2004 he was a Post-doctoral Researcher at LAAS (Laboratory for Analysis and Architecture of Systems), CNRS, Toulouse, France. Currently, he is a Professor at Institut MINES-TELECOM, Telecom SudParis, Evry, France. His main research interests are in the area of communication theory, non-linear signal processing and statistical image processing.